RICE UNIVERSITY

MEASUREMENT OF GAMMA RADIATION FROM THE CRAB NEBULA

by

DARWIN V. ELLIS

A THESIS SUBMITTED
IN PARTIAL FULFILLMENT OF THE
REQUIREMENTS FOR THE DEGREE OF

DOCTOR OF PHILOSOPHY
IN
SPACE SCIENCE

THESIS DIRECTOR

Robert C. Haymes

Houston, Texas

December, 1967

Table of Contents

I. Introduction

Gamma-ray emission from the Crab Nebula has been predicted on the basis of several distinct theories. The primary objective of the research described herein was to search for these gamma rays and thereby attempt to test some of the leading theories.

Since the discovery of extraterrestrial x-rays by Giacconi *et al.* (1962) the field of high-energy astronomy has rapidly expanded both in experimental and theoretical aspects; to date no single process can be identified with any of the observed fluxes of hard radiation. Also, gamma rays ($h\nu > 100$ keV) have never previously been detected from any discrete source beyond the solar system.

This thesis is concerned with adding to our understanding of both the nature of the supernova phenomenon and the nature of the x- and gamma radiation emitted by its remnants. It is for this reason that the Crab Nebula was chosen for study, as it is widely believed (Mayall, 1962) to be the remnant of the supernova of 1054 A.D. recorded by Chinese astronomers. In addition, the Crab is one of the brightest discrete radio objects. It is also one of the first discovered discrete celestial x-ray sources other than the sun.

The role of the supernova in astrophysics is perhaps very important as it is thought to be associated with the production and abundances of the elements. One current theory which attempts to deal with the nature of supernovae on this basis provides a primary motivation for the work described in this thesis.

A supernova is a star that has undergone a very

violent explosion. The luminosity increases sharply from normal to greater than 10^6 times the luminosity of the sun; it may in some cases become as bright as an entire galaxy ($10^9 L_\odot$). A number of these events have been recorded by astronomers over the last ten centuries. The observed supernovae seem to fall into two general classifications, based on their optical spectra. Supernovae of Type I are characterized by having light-curves and spectra which are very similar to one another. After the initial 20-30 day decline, the light curves show an approximately exponential decay. Their spectra consist of broad features that could represent emission, absorption, or both processes mixed; as of yet they have defied interpretation (Minkowski, 1964). Type II supernova light-curves decline faster than the exponential decay of Type I events, but the decay is somewhat irregular within the group. The spectral details of Type II events have been identified and have been found to be rich in iron and other metals. The kinetic energy of the ejected envelope for a Type II supernova is estimated to be on the order of 10^{52} ergs while that of a Type I is less by approximately four orders of magnitude (Shklovskii, 1960).

On the basis of three supernovae analyzed by Baade; Burbidge, Hoyle, Burbidge, Christy, and Fowler (1956) noted that the light curves for Type I events had half lives of 55 ± 1 days. They integrated the energy under the exponential portion of the light curve and found it to be about 10^{47} ergs. The exponential decay suggested to them that the source of the energy might be radioactivity.

A check of half-lives of radioactive nuclei presented

them with three candidates; Be^7, Sr^{89}, and Cf^{254} all have half-lives of 55 days. Each decay of Be^7 liberates a mean energy of 57 keV and the mean electron energy released by Sr^{89} is 600 keV. From this they determined the mass of the two nuclei required to produce the 10^{47} ergs. Taking a galactic rate of occurrence for Type I supernovae to be $(500 \text{ yr.})^{-1}$ they found that the abundances of Be and Sr would be about 100 times their observed values (Burbidge et al., 1956). However, Cf^{254} spontaneously undergoes fission and liberates 200 MeV/decay. This seemed plausible to them as the source for the supernova light-curve energy; only 6×10^{-4} solar masses of Cf^{254} would be required.

With these preliminaries Burbidge, Burbidge, Fowler, and Hoyle (1957)[1] went on to develop a rather complex theory of the role of the supernovae in nucleosynthesis. That a supernova is a likely site for nucleosynthesis follows from considerations of the high temperatures and pressures that probably occur in such explosions. This monumental paper summarized and greatly extended the knowledge of nuclear astrophysics. The portion dealing specifically with supernovae is referred to as the Californium-hypothesis and can be roughly described as follows.

In a supernova outburst considerable nucleosynthesis might take place through the r-process. The r-process is described simply as the rapid addition of neutrons to heavy seed nuclei such as iron, building heavier nuclei until no further neutrons can be bound stably. At this

---

1. hereafter referred to as B^2FH

point in the periodic table the nuclei must make a charge adjustment through beta decay. Thus this build-up is governed by the rate at which charge can be adjusted. However there should be a stopping point for this process since the beta-decay lifetimes become large as the atomic number increases. So the authors (B^2FH) reasoned that the r-process might terminate at the isotope Cf^{254} which is unique among its neighbors in undergoing spontaneous fission and has the required half-life of 55 days.

To lend a little credibility to this theory it must be noted that in 1952 Cf^{254} was observed to be produced in a thermonuclear test by the instantaneous irradiation of Uranium by an intense neutron flux (Fields et al., 1956). However a critical look at the Californium-hypothesis reveals a number of shortcomings.

A more recent review (Morrison and Sartori, 1966) of Type I supernova data shows that the half-lives of the light curves range from 40-80 days. It is difficult to assume that each supernova is so individual as to require different radioactive isotopes to provide the energy. However Hoyle and Fowler (1960) have suggested that a mixture of varying proportions of associated isotopes produced by the r-process could account for the varying half-lives. Also no efficient mechanisms for converting the Californium fission energy into visible light were presented by the authors (B^2FH). In addition, if one assumes the galactic rate of supernovae occurrence to be $(300\ yr.)^{-1}$ (Clayton and Craddock, 1965), the abundances of the associated nuclei produced through the Californium mechanism are about two orders of magnitude larger than the values observed in solar-system material. However,

the r-process is regarded as plausible by astrophysicists and it may still go on in supernovae even if the Californium-hypothesis is incorrect.

Assuming the validity of the Californium-hypothesis Clayton and Craddock (1965) applied it to the Crab Nebula. Using the relative abundances predicted by B^2FH, Clayton and Craddock calculated the many daughter products which should be present in the Crab 910 years after its explosion. They then made a listing of the gamma-emissions of the most abundant daughter products. From the assumed distance of 3500 light years from the earth to the Crab Nebula they calculated the fluxes of these gamma rays at the top of the earth's atmosphere. The majority of the gamma lines lie in the region of 50-400 keV. The observation of these lines provides a crucial test for the Californium-hypothesis of supernovae.

Without the knowledge of the correctness of the Californium-hypothesis it is impossible to interpret Type I supernovae light-curves unambiguously. It is also impossible to locate the site of the r-process which certainly must play an important role in nucleosynthesis.

A few alternate solutions have been proposed. One by the same authors (Hoyle, Fowler, Burbidge, and Burbidge, 1964) is based only on gravitational collapse and has nothing to do with radioactivity. However the authors state that they cannot decide between the two alternatives on the basis of theory alone and ask that an experiment be performed.

Anders (1959) has suggested that the exponential decline of Type I supernova light-curves is due to 45 day Fe^{59} rather than Cf^{254} and has in turn predicted a completely

different set of radioactive nuclei to be present in the Crab. However, the Crab may be expected to emit gamma radiation even if no radioactivity is present, by other mechanisms which have been proposed.

Morrison and Sartori (1966) have proposed a theory which attempts to explain all details of the visible supernova spectrum. They assume that the light observed is fluorescence excited by the initial ultra-violet continuum of the supernova incident upon the surrounding interstellar gas. As time passes the visible light is produced by gas farther from the supernova. The observed time variation is merely a reflection of the exponential attenuation of the ultraviolet as it moves outward in space. The heated gas also produces x- and gamma-radiation.

Finzi (1965) contends that the radial oscillations of a neutron star provide the energy for the observed light and he shows that the maximum vibrational energy of a neutron star is consistent with the 10^{47} ergs under the exponential portion of the light curve.

In the last few years a large number of x-ray sources have been discovered in addition to the Crab, but no satisfactory explanation of their nature has been found. Some of the models considered most frequently will briefly be mentioned here.

There are a number of basic processes by which energetic photons are produced:

1. Bremsstrahlung,

2. Compton scattering (sometimes referred to as the inverse Compton effect) of low energy thermal photons by high energy electrons, producing high energy scattered

photons,

3. Synchrotron radiation produced by electrons in magnetic fields,

4. The decay of π^o mesons following the production of mesons in collisions between cosmic ray particles and nuclei,

5. Characteristic x-rays from atomic transitions,

6. Annihilation radiation,

7. Formation of Deuterium via $n+p \rightarrow d+\gamma$ (2.23 MeV),

8. Nuclear gamma rays.

The processes most likely to be responsible for the cosmic x-ray sources are the first three listed (Burbidge, 1966).

In 1962 the first model suggested was that of a neutron star but now that appears untenable for several reasons aside from the possibility that stable neutron configurations may never be formed. For the Crab, the linear dimensions of the low-energy x-ray source are known from a lunar-occultation experiment to be on the order of 1 light year. This would require a cluster of neutron stars, since they are predicted to have radii as small as 10 km. It is difficult to imagine how such a cluster might be formed. Also, the high energy x-ray tail of the Crab doesn't fall off as fast as predicted by black-body radiation. Finally, the lifetimes of the neutron stars may be too short due to neutrino cooling (Bahcall and Wolf, 1965).

Synchrotron radiation may be a possible source but this too has its difficulties. The electron energies required to produce x- or gamma-ray emission are extremely high. In magnetic fields of the strength which are inferred

from the optical data to be present in the Crab, their radiative lifetimes are very short compared to the age of the Nebula. Also the total electron energy involved must be comparable to the energy released in a supernova outburst. However, it is possible to construct models of x-ray sources on the basis of the synchrotron radiation hypothesis. This has been done in some detail by Tucker (1967), but the spectral shape depends on the details of the acceleration, energy loss and trapping of the electrons.

An alternate model is one of a thin hot cloud which emits x-rays as part of the thermal bremsstrahlung. This x-ray production is efficient in a high temperature ($>10^7$ ^oK) and low density gas. Here the difficulty is to explain how a plasma is heated up to such a high temperature although radioactive heating (Morrison and Sartori, 1965) and shock heating (Heiles, 1964) have been suggested, as well as the postulated ionized atmosphere surrounding a neutron star.

These models will be considered more carefully in a later section in regards to our recent measurements.

II. Apparatus

A. Detector

As stated in the introduction the purpose of the experiment was to search for high energy radiation from the Crab Nebula; in particular to look for line gamma emission. Figure 1 reproduces the line spectrum estimated for the Crab by Clayton and Craddock (1965) and it was this theoretical spectrum that set the design criteria for the detector. Virtually all of the radiation is predicted to be in the energy range 50 keV to 400 keV with a maximum line strength of only 10^{-4} $cm^{-2}sec^{-1}$; photons of these energies can penetrate the earth's atmosphere to balloon altitudes ($\sim$3 - 4 g cm^{-2}) without serious attenuation.

For the measurement of such a spectrum a detector must meet the following requirements:

1) high efficiency for gamma ray detection in the range 50 keV to 400 keV,

2) sufficient energy resolution for making the spectral analysis,

3) directional detection capability,

4) rejection of other types of radiation such as charged particles.

The solution to this design problem has been detailed by Craddock (1967) but for the sake of completeness a brief summary will follow.

The detector chosen was a NaI(Tl) scintillation crystal 4 inches in diameter and 2 inches thick viewed by an RCA 8054 photo tube. This thickness provides good detection

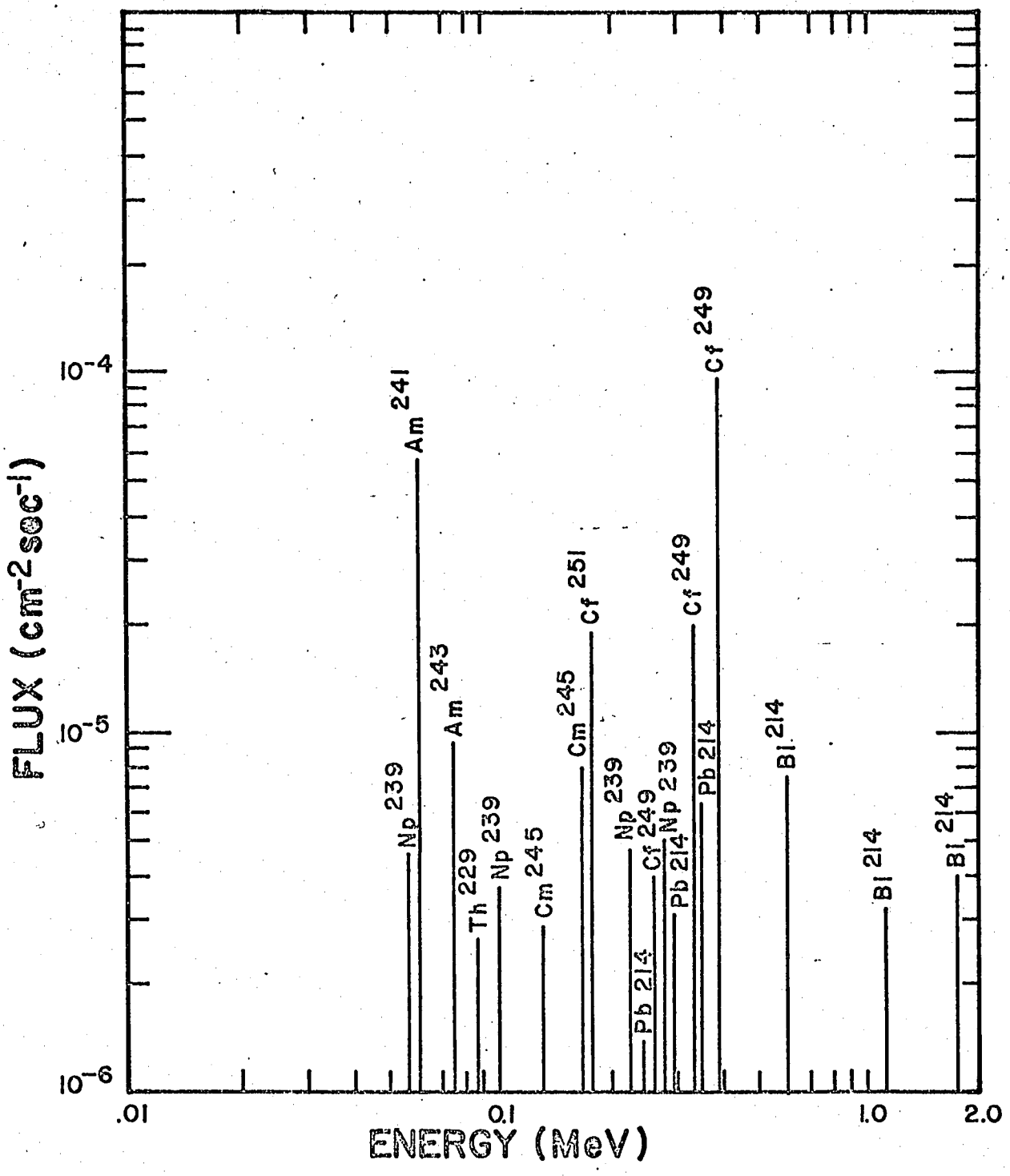

SPECTRUM OF LINE FLUXES ANTICIPATED FROM THE CRAB NEBULA

FIG. 1

efficiency in the region of interest. The efficiency for such a crystal as a function of energy is shown in Figure 2. The measured resolution of the flight crystal was 8.4% at 660 keV, FWHM.

Initially the spectrum of the background radiation to be encountered at balloon altitudes was unknown but as a design criterion it was estimated from the results of Arnold et al. (1962). These data were obtained from a nearly-omnidirectional phoswich on board the Ranger 3 and Ranger 5 spacecraft. This spectrum, assumed to be isotropic, yields a flux of about four orders of magnitude greater than the line fluxes expected from the Crab, when integrated over the energy range 50 keV to 400 keV. It is for this reason that a highly directional detector is desirable. Tight collimation is one way of improving the signal to noise ratio.

To obtain directionality, the central crystal was placed inside a NaI(Tl) collimator in the shape of a cylindrical cup. This arrangement is shown in Figure 3. The guard crystal is 12 inches long with a back thickness of 4 inches and an outer diameter of 9.5 inches. The two crystals are optically decoupled. The directionality is enhanced, in addition to the shielding, by the use of anticoincidence techniques. Six photomultipliers view the guard crystal and are in anticoincidence with the output of the central photomultiplier. A 1/4 inch thick plastic scintillator covers the aperture of the detector to complete the 4π anticoincidence shielding for charged particles. An event detected in the central crystal is counted only if it is not accompanied by a pulse from the

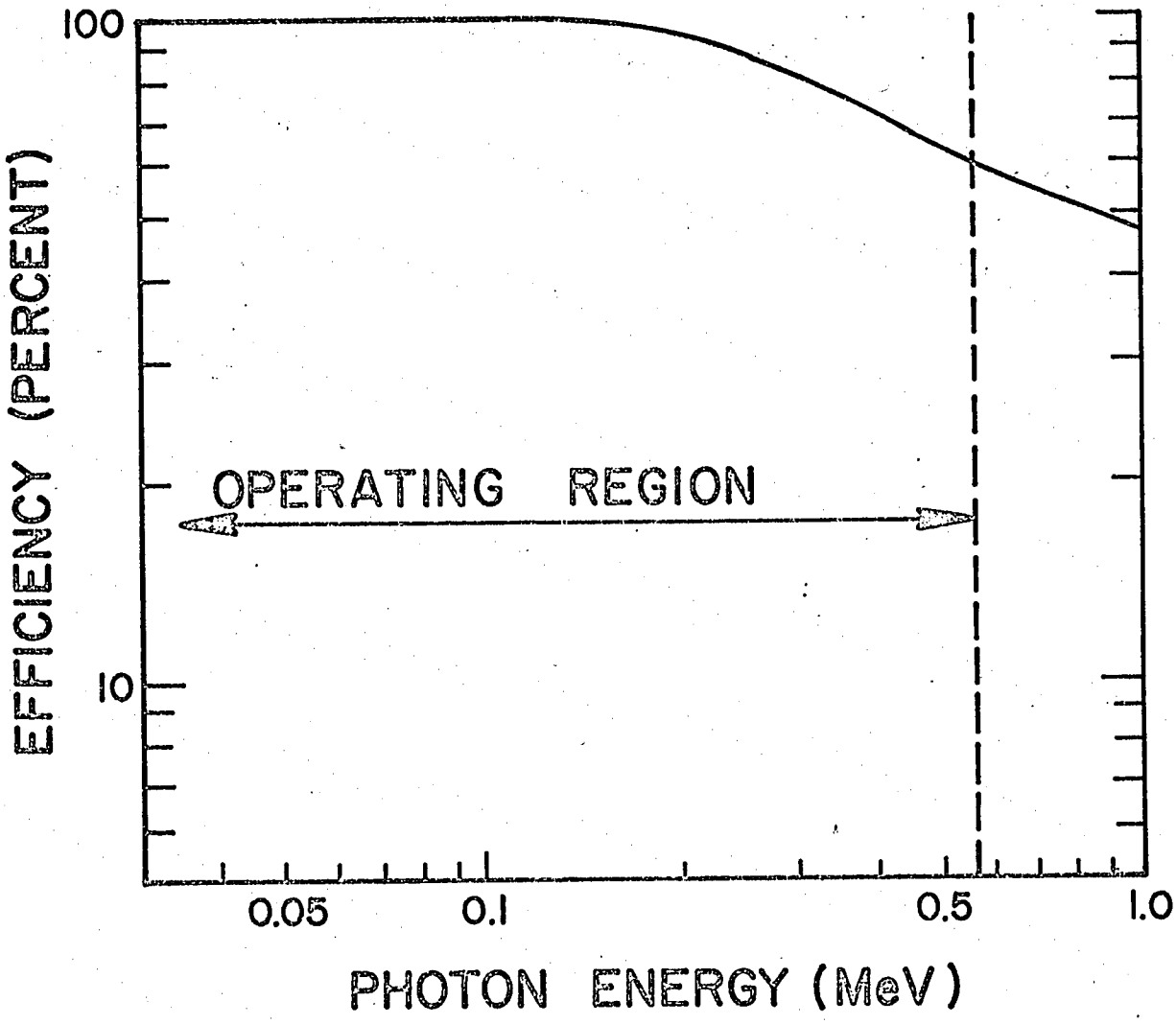

ENERGY DEPENDENCE OF
DETECTION EFFICIENCY

FIG. 2

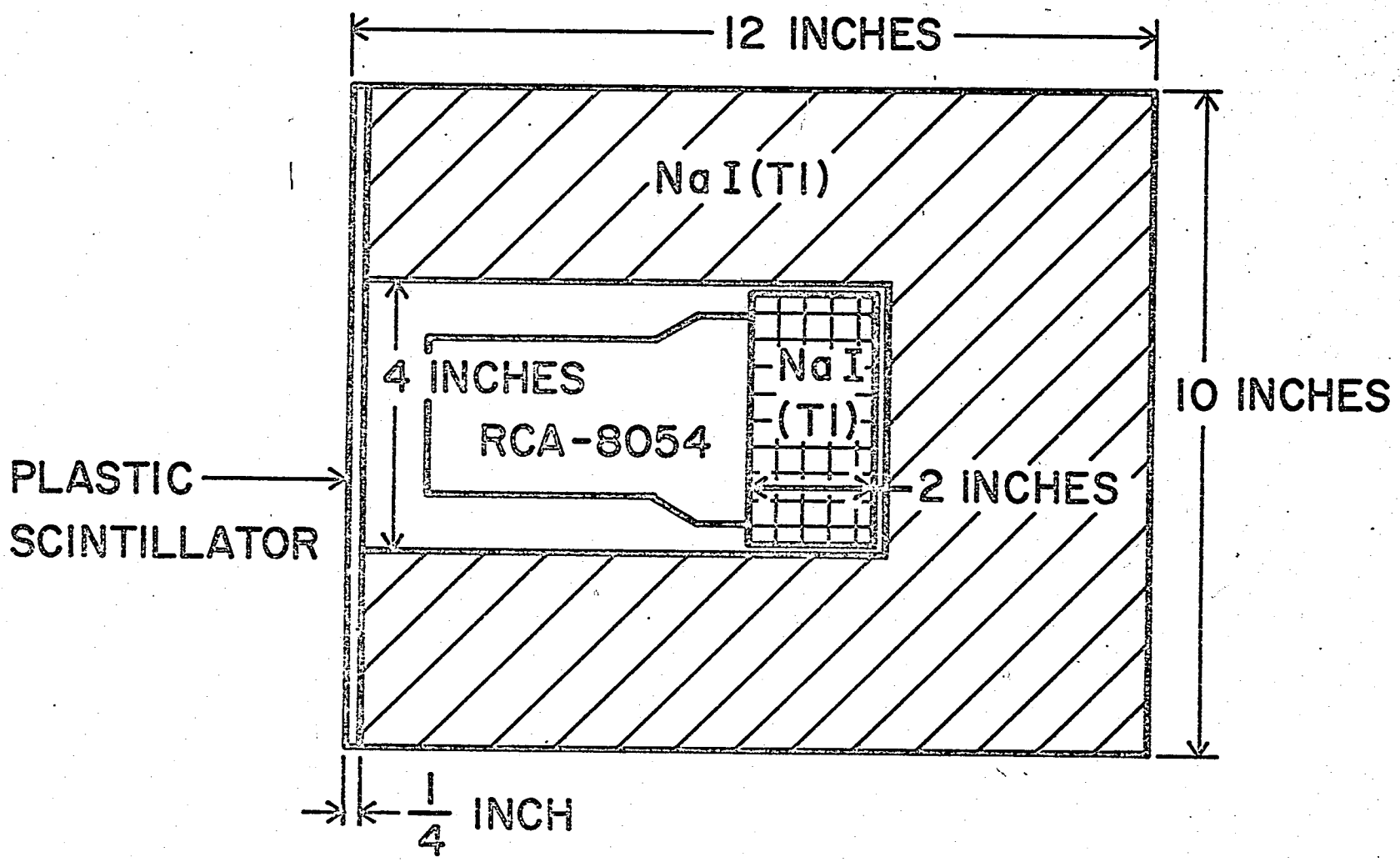
12 INCHES
NaI(Tl)
4 INCHES
RCA-8054
NaI
(Tl)
2 INCHES
10 INCHES
PLASTIC
SCINTILLATOR
1/4 INCH

FIG. 3

guard crystal or plastic scintillator.

In the configuration shown in Figure 3 the half-flux angle for a point gamma source is approximately 12° from the axis. Tighter collimation from the use of more NaI would lead to prohibitive expense. The angular response of the detector at two representative photon energies is shown in Figure 4.

In addition to the gamma ray detector, an automatic ionization chamber was on board during the flight. The ionization chamber gives a measure of the intensity of the ionizing radiation. With this it was possible to independently monitor the stability of this radiation. Presumably this radiation indirectly produces, at least a portion, of the observed gamma ray "background" spectrum which is present at balloon altitudes. This instrument has been described in detail by Neher (1953) and Neher and Johnson (1956).

B. Pointing System

A stable platform must be provided for the directional detector described in the preceding section. The platform must have tracking capabilities so that a celestial source may be observed for as long a time as practical at balloon altitudes.

The detector mount is a modified equatorial system. The declination axis is fixed so that there are only two degrees of freedom; the right ascension axis and the azimuth axis. The usefulness of an equatorial mount, once the polar axis is set for the latitude of the observer and the declination axis set for the declination of the source, is that to track a celestial object the detector must

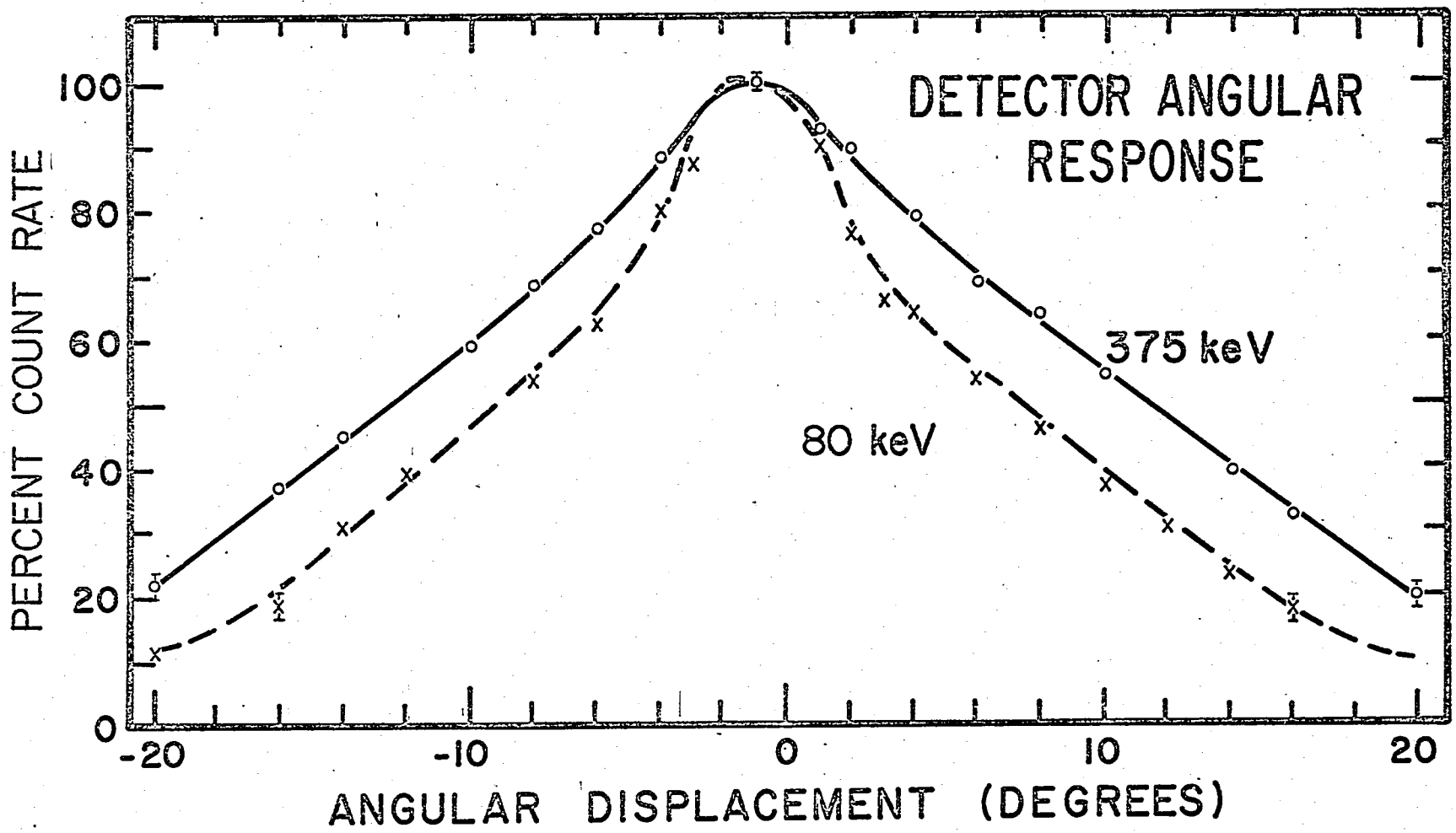
DETECTOR ANGULAR RESPONSE
375 keV
80 keV
PERCENT COUNT RATE
100
80
60
40
20
0
-20
-10
0
10
20
ANGULAR DISPLACEMENT (DEGREES)

FIG. 4

just revolve about the right ascension axis at the sidereal rate. This rotation is provided by a 60 Hz synchronous motor and a suitable gear train. A circuit on board the gondola provides stable 60 Hz power for the motor.

The azimuth drive is provided in order to keep the right ascension axis parallel to the earth's spin axis since the outer gondola is free to rotate with the balloon. It is powered by a 150 watt dc torque motor and is controlled by a magnetometer servo system. The magnetometer measures the horizontal component of the earth's field and is rigidly attached to the support structure for the polar axis (referred to as the inner gondola). Its orientation is fixed such that a stable null is provided by the torque motor when the right ascension axis is pointed to true North. The torque motor on the inner gondola turns against an inertia wheel or outer gondola (an aluminum framework measuring 9 ft. by 9 ft.). Additional inertia is obtained from the semi-rigid coupling of the outer framework to the balloon. A schematic diagram is shown in Figure 5.

The inner gondola, in addition to providing the mount for the detector, also houses all the electrical systems of the experiment. This includes a pressurized box containing the silver-cell battery packs.

Tests in the laboratory and photographs taken of the position of the sun during various flights have shown the pointing accuracy to be about 1^{o} in azimuth. This is quite satisfactory for the type of work done in this experiment. This can be seen from the following argument.

The separation angle γ, for a source at zenith angle Z, (see Figure 6) is given by;

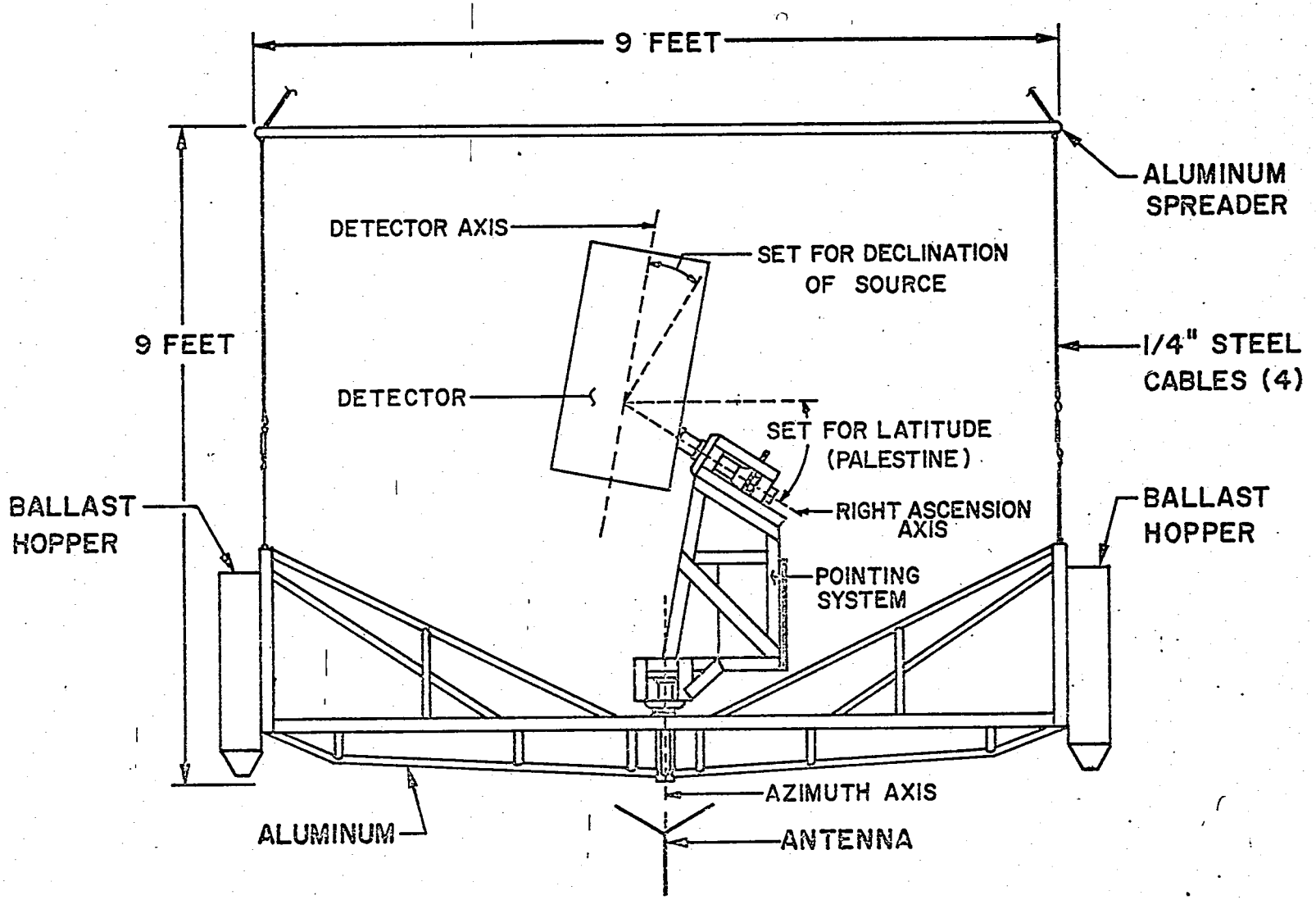

BALLOON BORNE SYSTEM

FIG. 5

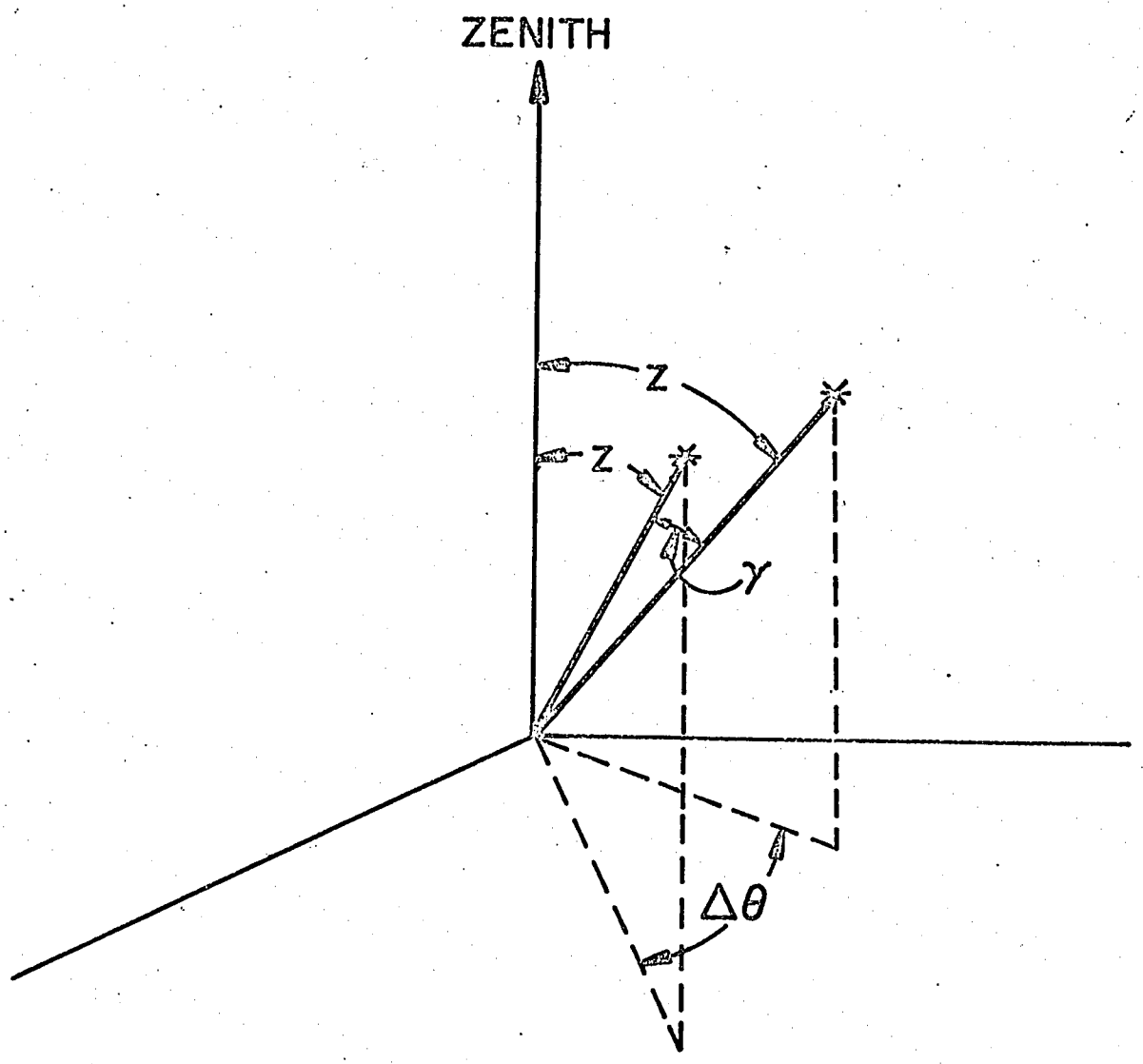

FIG. 6

$$\cos \gamma = \cos^2 Z + \sin^2 Z \cos (\Delta\theta),$$

where $\Delta\theta$ is the error in the azimuth pointing. The graph in Figure 7 shows the insensitivity of the pointing accuracy on the azimuth error, $\Delta\theta$, as a function of the zenith angle. Since the experiments are performed for values of $Z < 50^\circ$ to minimize the effect of atmospheric absorption, the azimuth error can be quite large and still keep the source within the 12° half-flux angle of the detector. For example, at a zenith angle of 45°, usually the maximum zenith angle for our observations, the azimuth error can be as large as 20° and the detector will still be pointed within 14° of the source, while at a zenith angle of 20° the azimuth error can be as large as 42° for the same angular separation. Thus the greatest source of tracking error can arise from the initial setting of the right ascension; this will be discussed in section F.

Figure 7 also gives an insight to the problem of obtaining background observations at small zenith angles. For observations around transit it is difficult to obtain a sufficient separation from the source unless the azimuth is offset by 180°. Even this is not satisfactory for cases of celestial objects with declinations between 26° and 38° when observing at latitudes of 32° (Palestine, Texas) with a telescope of a 12° half-angle. In such cases the maximum obtainable source separation during offset at transit cannot reach the required minimum of 12° and thus no background observations are obtainable during these times with the present pointing system. Fortunately the declination of the Crab is 22° so that the minimum source separation is about 20° at transit.

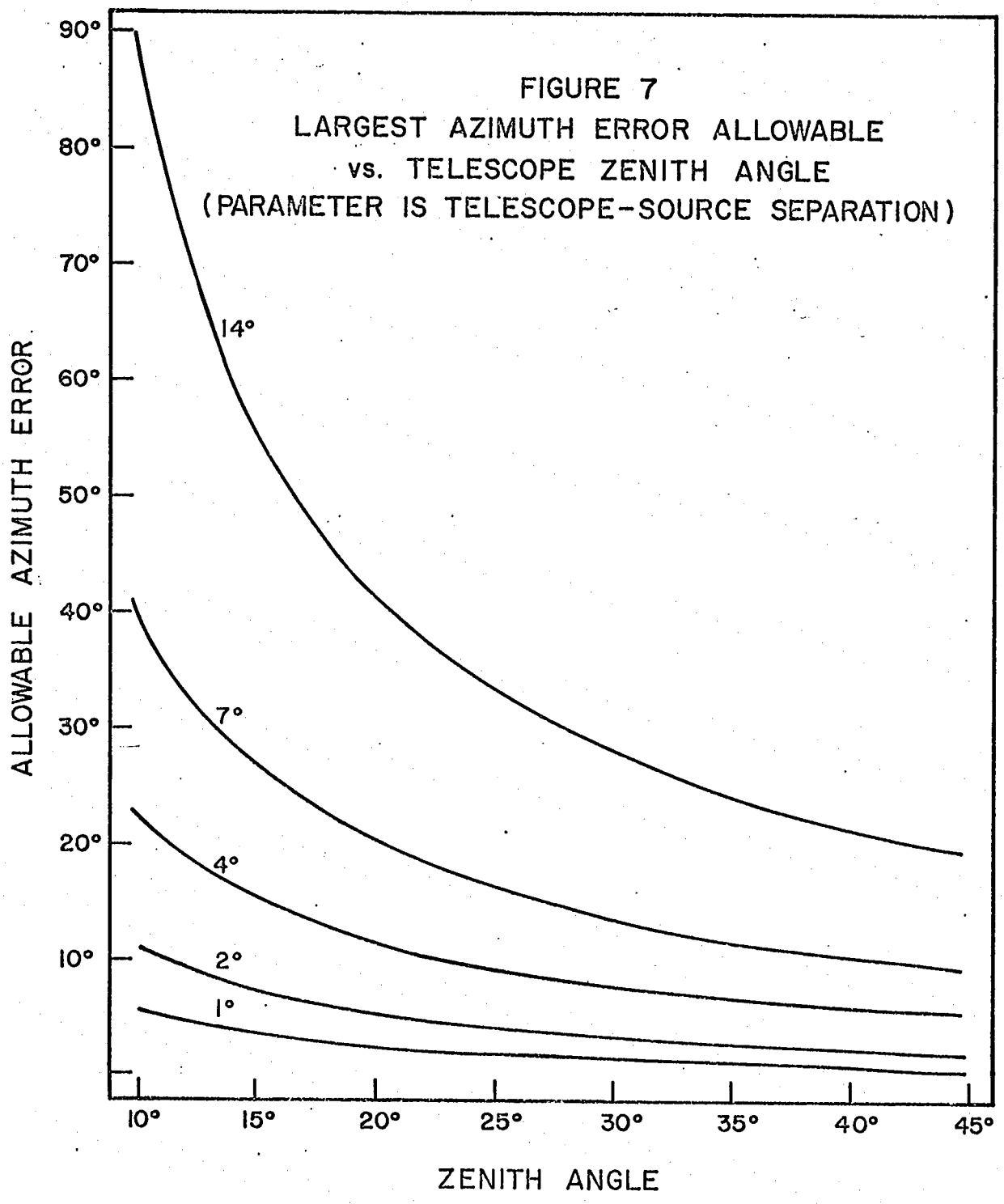
FIGURE 7
LARGEST AZIMUTH ERROR ALLOWABLE
vs. TELESCOPE ZENITH ANGLE
(PARAMETER IS TELESCOPE-SOURCE SEPARATION)
ALLOWABLE AZIMUTH ERROR
90°
80°
70°
60°
50°
40°
30°
20°
10°
14°
7°
4°
2°
1°
10°
15°
20°
25°
30°
35°
40°
45°
ZENITH ANGLE

The insensitivity of pointing accuracy on azimuth error is helpful in setting the magnetometers prior to the flight. In the course of a flight the balloon may drift up to 700 or 800 miles and thus the local magnetic declination might change five or six degrees. For the most accurate pointing the direction and speed of the high altitude winds are provided by the U. S. Weather Bureau before a flight. With this information the magnetometers can be set for a magnetic declination corresponding to the estimated midpoint of the trajectory. In this way the error associated with the magnetic declination can be reduced to be a maximum of two or three degrees. With reference to Figure 7 this is seen to be tolerable even at zenith angles of 40°, since the pointing of the telescope will be within 2° of the source (computed for the Crab Nebula).

Since the angle which the right ascension axis makes with respect to horizontal, is rigidly fixed and set for the latitude of Palestine, Texas there is no possibility of making corrections for latitude drifts during a flight. This is a minor problem, however, since the majority of flights conducted by the National Center for Atmospheric Research (NCAR) have exhibited trajectories that were within $\pm 2^{\circ}$ of the launch latitude. Since the speed and direction of the high altitude winds are known pretty well in advance of flights, a launch can be ruled out if the wind directions are significantly different from due East or West.

For this flight there existed command capability for changing the azimuth pointing by 180° (i.e., to due South) periodically so that background measurements could be made.

In addition there were commands to control the speed of the right ascension drive system.

C. Electronics

The detector-associated electronics consist basically of three types; high voltage supplies, reject circuitry, and the pulse height analyzer. The power supplies convert the nominally 28V dc gondola supply voltage into stable high voltages. Great care was taken in the design and construction of the high voltage supplies so that temperature and input voltage variations had a minimal effect on the output voltage. Three separate power supplies were used for the photomultipliers on the main crystal, plastic scintillator, and the well crystal.

The reject circuitry compared the summation of the outputs of the phototubes viewing the well crystal and the plastic scintillator to the output of the central multiplier. If the two outputs have simultaneous pulses (within 2 μsec.) the analyzer is blocked and the pulse from the central tube is not analyzed.

If a bona fide pulse is received by the analyzer it is converted to a segment of 1 MHz oscillations by the pulse height to time converter; the number of cycles being proportional to the height of the pulse and in turn to the energy of the incident photon. An accumulator then classifies a pulse as being in one of 127 channels or pulse-height windows and the contents of the accumulator are serially read out onto the telemetry at a 5 kHz rate. Pulses exceeding the upper energy limit (approximately 560 keV in this experiment) are all labeled as channel

number 128.

To operate the right ascension synchronous motor an ac to dc converter is required. It produces power at a stable frequency over temperature and input voltage variations. In addition the ac-dc converter is required to change from the normal 60 to 120 Hz upon radio command for adjustments in the right ascension tracking; it can also be temporarily stopped for the same purpose.

The entire gondola was thermally insulated before the flight and the detector and its associated electronics were wrapped with heater strips and then insulated with "Pleogen" foam. These heater strips were thermostatically operated to keep the detector and electronics at a constant 80 ± 1°F during the flight in order that the effect of temperature changes be minimized.

The power for the majority of the system was supplied by three Yardney silver-cell battery packs. The main pack of 70 Amp-hr. batteries was nominally at 28V, while the heater pack of 40 Amp-hr. batteries was at approximately 35V. The command receiver utilized a pack at -12V.

A block diagram of the entire electrical system is shown in Figure 8.

D. Telemetry

An eight-channel FM/FM telemetry system was used for data transmission. The system employed a 2-watt transmitter operating at 253.8 MHz and a spare transmitter on 234 MHz. The command system allowed the telemetry to be switched onto the spare transmitter in the event of the failure of the primary transmitter. The eight channels were provided by voltage controlled oscillators (VCO)

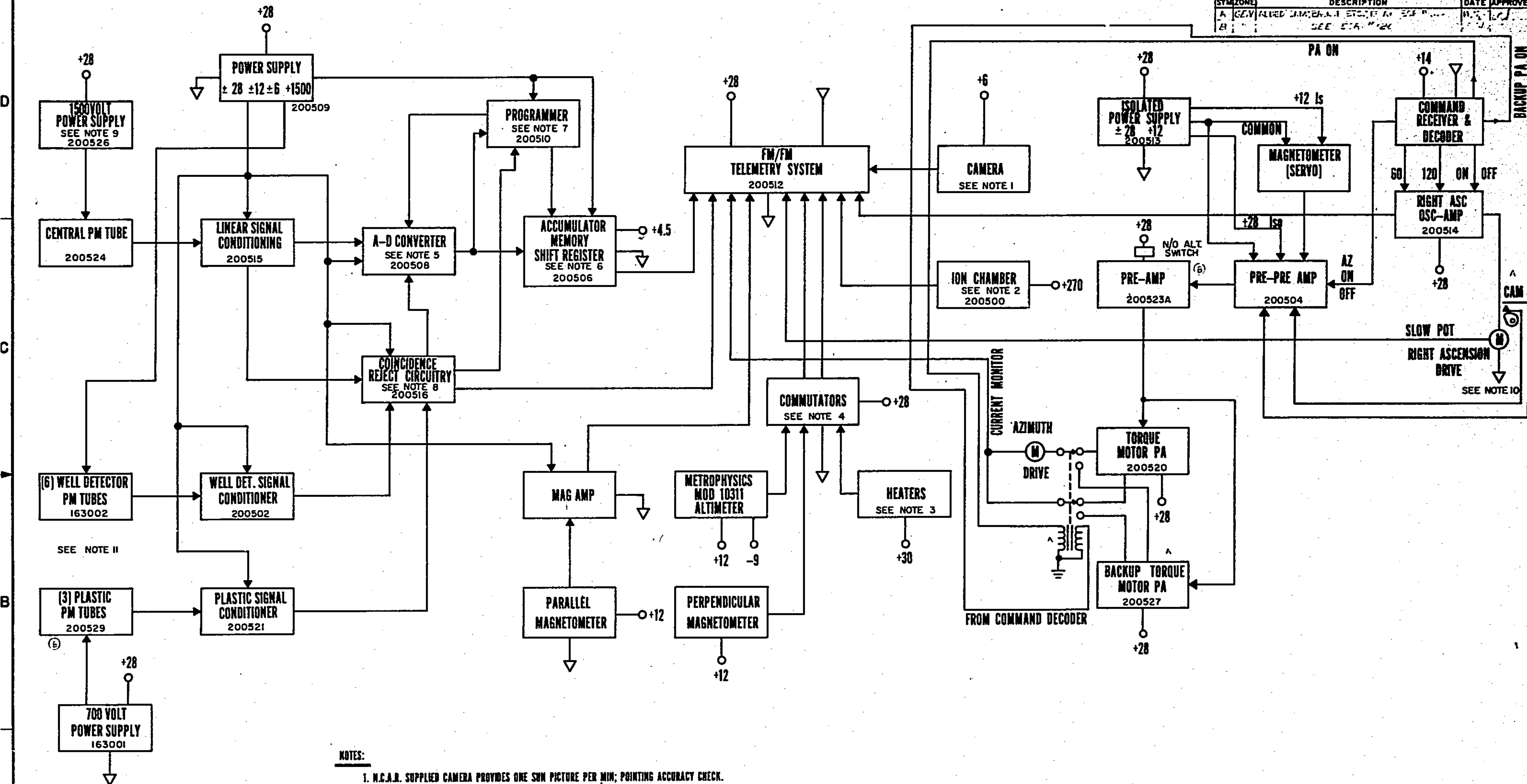

NOTES:

1. N.C.A.R. SUPPLIED CAMERA PROVIDES ONE SUN PICTURE PER MIN; POINTING ACCURACY CHECK.
2. ION CHAMBER MONITORS COSMIC RAY INTENSITY.
3. THERMOSTATS SET FOR 80°F;CONTROL DETECTOR TEMPERATURE;270 WATTTS MAX;1.2 KWATT.
4. COMMUTATORS A & B PROVIDE 40 CHANNELS OF HOUSEKEEPING DATA.
5. A/D OPERATES AT ONE MEGACYCLE.
6. ACCUMULATOR CLASSIFIES PULSE HEIGHT INTO ONE OF 127 CHANNELS ;CH. 128 CONTAINS OVERFLOWS.
7. PROGRAMMER PROVIDES 5KB/S DATA-RATE FOR TLM.
8. ONLY CENTRAL PMT PULSES NOT COINCIDENT WITH OTHERS ARE PASSED TO A/D ; RESOLVING TIME ~ 100 NSEC.
9. ADJUST HV FOR OPTIMUM GAIN AND RESOLUTION.
10. CAM MOUNTED ON R.A. DRIVE MOTOR PROVIDES 180° AZIMUTH REVERSAL EVERY 11 MINUTES.
11. REFER TO DWG NO. 200528 FOR DETECTOR.
12. MAGNETOMETERS ARE SCHONSTEDT RAM 5C.

QTY REQD	ITEM NO.	NOMENCLATURE OR DESCRIPTION	PART OR IDENTIFYING NO.	MATERIAL OR NOTE	ZONE	UNIT WT

LIST OF MATERIALS OR PARTS LIST

DO NOT SCALE PRINT

UNLESS OTHERWISE SPECIFIED DIMENSIONS ARE IN INCHES WITH TOLERANCES ON: FRACTIONS ± 1/32 DECIMALS .XX ± .02 .XXX ± .005 ANGLES ± 0°15'

MATERIAL ~

FINISH REQD ~

SPACE SCIENCE FACILITIES
RICE UNIVERSITY HOUSTON, TEXAS

GAMMA SCOPE
SYSTEM BLOCK DIAGRAM

SIZE D 200525 B

SCALE ~ SHEET 1 OF 1

operating on IRIG subcarrier frequency channels 9 through 15 and H (3.9, 5.4, 7.35, 10.5, 14.5, 22.0, 30.0, and 165 kHz). Table I shows the functions of each channel.

TABLE I

IRIG Channel	Center Frequency (kHz)	Data
9	3.9	Commutator A
10	5.4	Torque motor curren
11	7.35	Commutator B
12	10.5	R.A. drive monit. + ion chamber
13	14.5	R.A. frequency
14	22.	Parallel magneto-meter
15	30.	Reject rate
H	165.	PCM

Most of the housekeeping information (battery voltages, high voltage monitors, state of pressurization indicators and heater status) were commutated on channels 5 and 7. The commutators used had 20 available positions and completed a cycle every five minutes. Table II gives the telemetry format for the two commutators.

TABLE II

Commutator A Position Number		Commutator B Position Number	
1.	Ground	1.	Ground
2.	+2.5 v	2.	+2.5
3.	+5.0 v	3.	-2.5
4.	Perpendicular Magnetometer	4.	R.A. Drive Freq.
5.	Perpendicular Magnetometer	5.	R.A. Drive Freq.
6.	Battery Temp. Monit.	6.	R.A. axis Monit.
7.	H.V. Monit. (Detector)	7.	R.A. axis Monit.
8.	H.V. Monit. (Guard)	8.	Mag. Power Supp.
9.	H.V. Monit. (Plast.)	9.	Bearing Thermostat
10.	Volt. Monit. (Main pack)	10.	Power amp. Thermostat
11.	Volt. Monit. (Heater pack)	11.	
12.	Volt. Monit. (4.5 v pack)	12.	
13.	Torque Motor Current	13.	thermostats
14.	Perpendicular Mag.	14.	
15.	Perpendicular Mag.	15.	
16.	Press. Monitor Batt. Box	16.	-12v monitor
17.	Press. Monitor Elec. Can	17.	
18.	Press. Monitor Detector	18.	
19.	Press. Monitor H.V. supplies	19.	command radio
20.	Press. Monitor R.A. Drive	20.	

The calibration of the telemetry was critical only for three channels (9, 11, 14), since the other channels carried digital data or analog data for which a relative change was all that was required to determine the condition of the system being monitored.

The calibration of channels 9 and 11 was facilitated by reference voltages provided in the first three positions of the commutator sequence. These voltages were tapped from the pulse height analyzer power supply and were stable to within 0.05 V over input variations from 24 to 34 V. The output of the channel 14 discriminator was calibrated during the setting of the magnetometers prior to the flight.

On playback the output of the channel 14 discriminator can be recalibrated during the ascent portion of the data. During that time the azimuth pointing system is not operating so that the gondola is free to follow balloon rotations. Consequently when it passes through due East or due West (i.e., the maximum output voltage) the output of the discriminator is adjusted to the previously determined output voltage, if it has drifted.

E. Data Acquisition and Recording

The FM telemetry system used is limited to line-of-sight reception. In practice this is between 400-450 miles at balloon altitudes. Consequently, for long duration flights two receiving stations are necessary if the high altitude wind speeds are in excess of 40 knots. These are provided by NCAR in the form of a launch site and telemetry station at Palestine, Texas and a mobile trailer which is located downwind according to the direction and speed of the high altitude winds.

A block diagram of the receiving station is shown in Figure 9. All the data plus a WWV time signal are recorded on four tracks of magnetic tape.

To provide live-time display and data reduction, a commercial pulse height analyzer (Nuclear Data) is used. The decoder bypasses the analog to digital converter (ADC) in this machine and utilizes only its storage and display. The decoder also differentiates the output of the channel H discriminator for tape recording and on the play-back it reconstructs the spectrum.

During a flight many telemetry items are monitored continuously. These include the magnetometer output, the commutators and the ion chamber; they are presented on strip chart recorders. The pulse code modulation (PCM) data is monitored on an oscilloscope display so that corrections can be made for any signal drop-out, and a digital counter continuously monitors the level of the reject rate.

F. Flight Preparations

The primary tasks involved in preparing the detector for flight are: 1) energy calibration, 2) determination of the gamma ray axis, 3) magnetometer positioning, and 4) setting of the initial hour angle.

The energy calibration was easily made by the use of the four radioactive sources: Se^{75}, Sn^{113}, Ba^{133}, and Na^{22}. These provided seven gamma-ray lines of known energies between 30 keV and 511 keV. The energy calibrations were made with the heaters on and through the telemetry system. The calibration curve for the flight described in this work is shown in Figure 10.

The determination of the gamma ray axis is a necessary

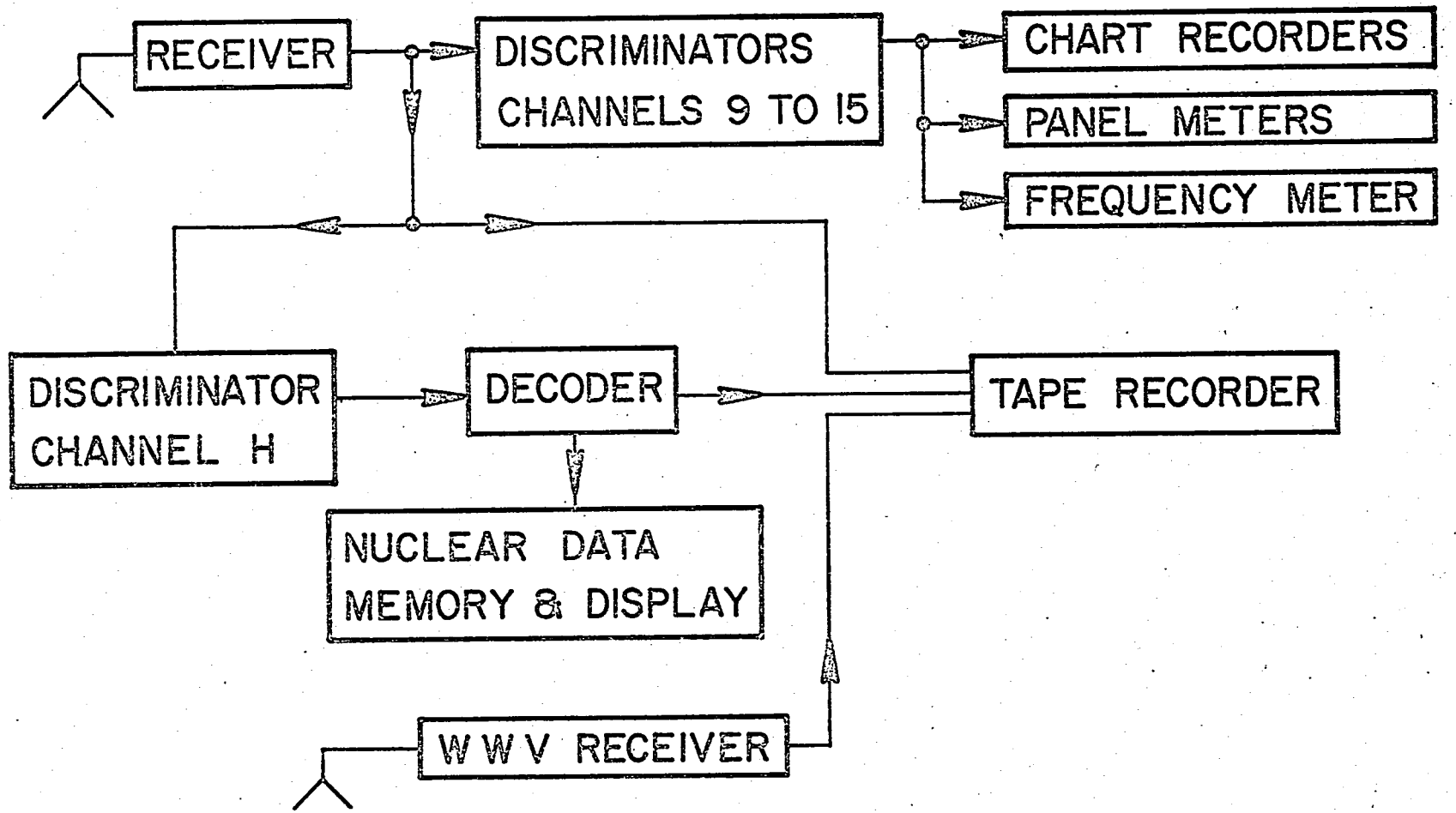

RECEIVING AND RECORDING SYSTEM

FIG. 9

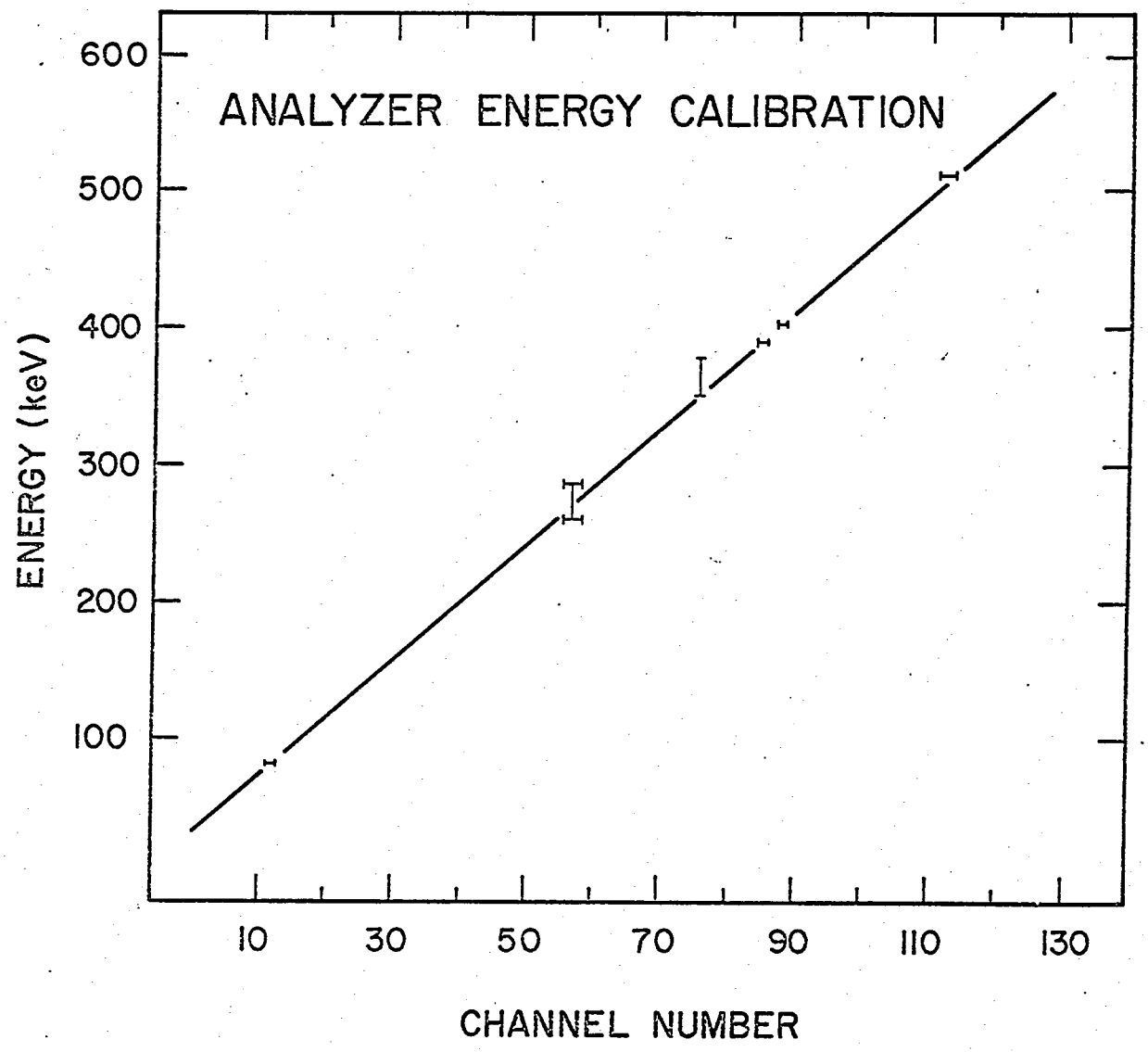
ANALYZER ENERGY CALIBRATION
ENERGY (keV)
600
500
400
300
200
100
10
30
50
70
90
110
130
CHANNEL NUMBER

FIG. 10

part of setting the magnetometers and the hour angle. To do this the telescope was placed in an approximately horizontal position and at a distance of about 15 ft. a grid of 2^{o} squares was laid off in the general field of view of the detector. The counting rate for a single line gamma source was determined at the intersections of the grid. By successive approximations it was possible to locate the gamma ray axis to within 1/2 degree.

When this point (the intersection of the γ-axis with the grid) had been found, a small sighting telescope mounted on the side of the detector, was adjusted so that its optical axis was parallel to the gamma ray axis. With the sighting telescope so oriented it was a simple matter to adjust the detector to a true horizontal position by the use of a surveyor's transit and rod.

At a latitude of 32^{o} the Crab ($\delta = 22^{o}$) crosses the horizon (Crabrise) at an angle of 25^{o} North of true East. This fact was used in setting the magnetometers. First an area free of magnetic anomalies was chosen in a field far from any surrounding metallic buildings. This was verified by sighting Polaris with the transit during one of its meridian passages and then measuring the magnetic declination ($\sim 8^{o}$ East) which agreed with that given in the current U.S.C.G.S. Aeronautical Chart for the Palestine area.

Once true North was found it was an easy matter to survey a series of angular displacements from a starting point at a heading of 65^{o} East. These were marked with stakes in 10^{o} increments extending $\pm 90^{o}$ from the starting point and at a distance of approximately 100 feet.

After these preparations the apparatus was brought

out into the field and placed in the center of this surveyed semi-circle and placed in a level attitude. The servo magnetometer was then rotated on its mounting bracket until it produced a stable null such that the starting-point stake was visible in the sighting telescope. Since the angles in the construction of the gondola were fixed for observation of the Crab at latitude 32^{o} then at this point the right ascension axis was parallel to the earth's spin axis. With the servo magnetometer permanently oriented on its mount, the inner gondola was rotated about the azimuth axis to the various surveyed positions and the readings of the two monitor magnetometers were noted. A typical calibration for these is shown in Figure 11. The two monitor magnetometers were placed in the horizontal plane perpendicular to one another to eliminate the ambiguity that results when only one is used.

The above description is for the case of no change in magnetic declination being taken into account. However, if the balloon were expected to drift through six degrees of magnetic declination, then the whole surveyed semi-circle would have been rotated by three degrees to minimize the pointing error during the flight. As previously noted, the precise amount of the rotation depends on a trajectory forecast.

The final arrangement is that of setting the telescope on the right ascension axis. From the American Ephemeris and Nautical Almanac (1967), the transit or zenith crossing of any celestial object over Palestine, Texas can be computed for any given day. Since the time from the horizontal position to transit for the Crab is $7^{h}05^{m}$, the telescope was usually left in the horizontal

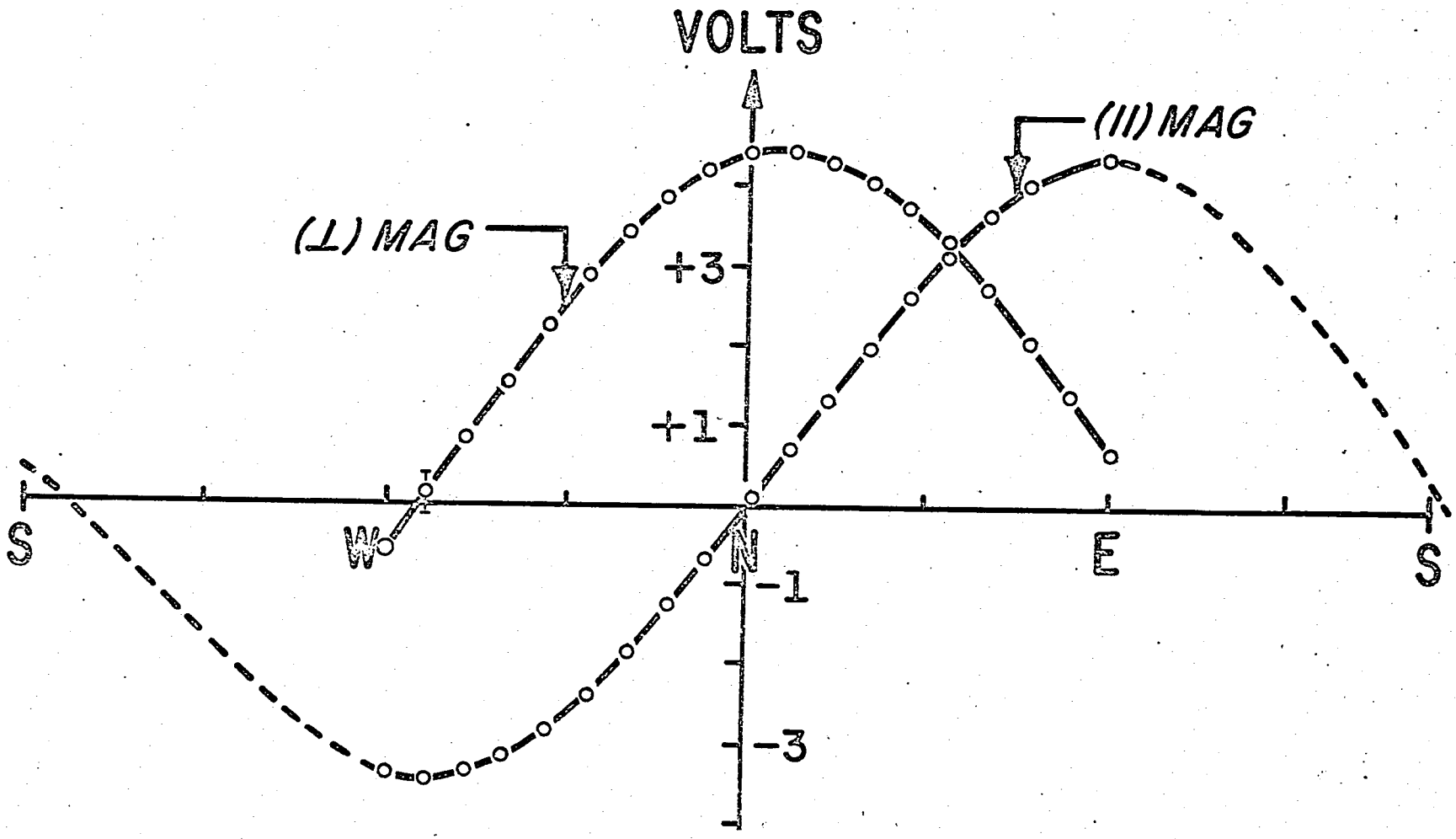

MAGNETOMETER CALIBRATION

FIG. 11

position for the launch. Since a typical daytime ascent to 130 thousand feet takes three hours, the telescope is then about four hours from transit upon reaching altitude for this configuration. For zenith angles greater than this ($\sim 45^{\circ}$), the atmospheric absorption becomes too large for usable data. The exact time of the turn-on of this motor varied and depended on the day of the launch.

Since the hour angle is computed for the longitude of Palestine, if any drift in longitude occurs then this setting is no longer valud. For this reason we had command capability to double the hour angle drive speed or to completely stop the drive. For a westward drift the drive was stopped four minutes for each degree of longitude crossed and for eastward drifts its drive rate was doubled for four minutes. Information on the position of the balloon was provided initially by radar and an automatically tracking receiver at the Palestine base, but for distances greater than 200 miles the tracking aircraft relayed the positions.

III. Results

A. Experiment

The balloon was launched from Palestine, Texas at 0615 CDT, 4 June 1967, and reached ceiling at approximately 0900 CDT. The pressure altitude, as indicated by a photobarograph, varied between 3.65 mb. and 3.35 mb. during the 7-3/4 hours that the balloon floated at ceiling. Termination occurred by radio command at 1634 CDT.

The method of the experiment was to drive the detector about the polar axis continuously at the sidereal rate, so that it would track the Crab in hour angle. In addition the polar axis was offset in azimuth by 180° every 10.5 minutes, after the servo system was turned on by radio command at 0913. The detector thus alternated between Crab and background measurements. Such a large offset angle was necessary for observing times near Crab transit. As mentioned previously, the Crab makes a transit at only 10° from the zenith at a latitude of 32°N, so that a large azimuth variation is required to keep the nebula well beyond the 12° half-flux angle of the telescope during the background measurements. During the background observations, no known discrete x-ray sources were in the field of view. In Figure 12 is shown the region of the sky scanned during the background observations. The offset pointing positions are marked in half-hour intervals measured from transit.

The ten minute observation technique assures us of having reliable background segments for each source observation period. It reduces the possibility of obtaining ambiguous data if the background flux suffers sudden,

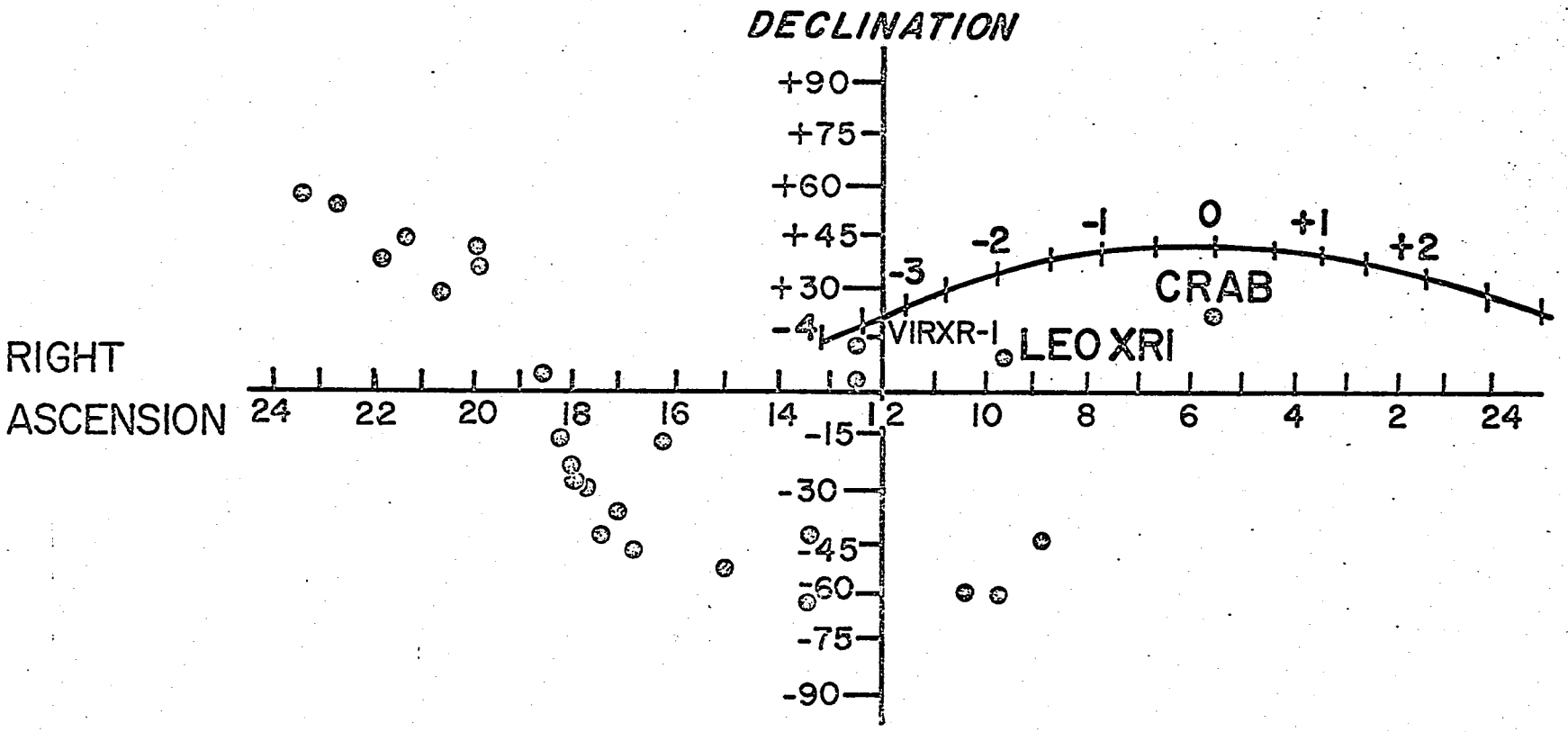

OFFSET POINTING CHART

FIG. 12

short term variation as well as compensating for slow changes in the background, such as those caused by changes in the zenith angle and in the latitude.

At approximately 1400 CDT, six minutes prior to Crab transit, the azimuth pointing system failed. After this time, there was no control over the azimuth of the detector; it was free to follow balloon rotations.

B. Solar Gamma-Rays

On the day of the flight the separation between the Crab and the sun was only $11\text{-}1/2^{\circ}$. Consequently during the Crab observation periods the sun was somewhat in the field of view. Since the sun is known to be an emitter of soft x-rays this factor must be considered in evaluating the data. It must first be noted that no x-rays in excess of 10 keV have, to date, been detected from the quiet sun. There have been, however, several reports (Peterson and Winkler, 1959; Chubb, Friedman, and Kreplin, 1960) of high energy radiation (20 keV to 500 keV) accompanying an Importance 2+ or Importance 3 solar flare.

The weekly summary issued by the ESSA Space Disturbance Forecast Center (SDFC) at Boulder, Colorado on 9 June showed only a small magnetic storm on 5 June and a small flux of low energy solar protons on 6 June as the two active events for the week 2-9 June. This is also in accord with the observation (CRPL, 1967) that no unusual geomagnetic or solar activity occurred on 4 June. The planetary magnetic index, K_p, varied between 1- and 4- during the flight.

In addition, the ionizing radiation background was independently monitored in flight by an ionization chamber

kindly loaned to us by Prof. H. V. Neher of the California Institute of Technology. The rate of ionization is shown in Figure 13. The ionization rate observed corresponds quite closely to data taken by Neher (1967) in the 1965 period of the quiet sun at these magnetic latitudes. We conclude that this result taken along with the CRPL and SDFC data, indicates that the observation took place during an undisturbed time.

The most recent and comprehensive search for quiet-time solar gamma rays has been made by Peterson, Schwartz, Pelling, and McKenzie (1966), in the energy range of 20 keV to 10 MeV. These data are plotted in Figure 14. It should be noted that this curve represents an upper limit. The flux expected (Peterson et al. 1966) from the solar albedo, presumably caused by cosmic rays, is also shown and lies several orders of magnitude below this experimental upper limit, in the energy range of our measurements. The dotted line represents the flux contribution that would have been detected by our instrument if indeed the sun were steadily emitting at a rate equal to this upper limit. Since this curve lies at least an order of magnitude below our measurement for the Crab, we conclude that any solar flux is negligible, compared to the flux which we have detected from the Crab.

C. Gamma Ray Spectrum of the Crab Nebula

Figure 15 shows a time-history of the flight. In the various energy-intervals, the segments of data due to the Crab and due to the background observations are apparent from the changes in counting rate. The flux is considerably enhanced each time the detector swings

ION PAIRS / SEC-CM^3 - ATMOSPHERE OF STP AIR
55
50
45
40
0800
1000
1200
1400
1600
TIME (C.D.T.)

FIG. 13

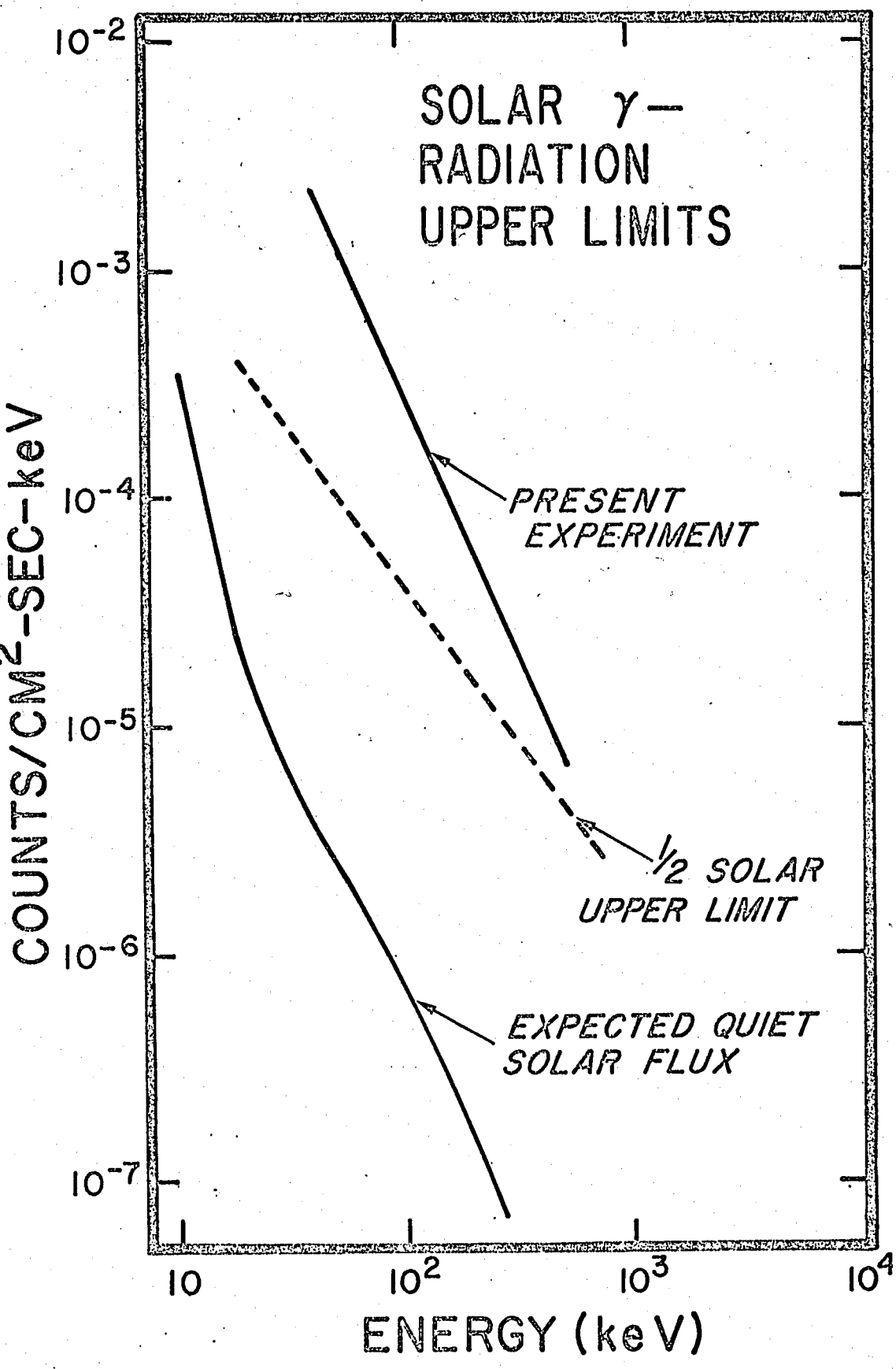
SOLAR γ-
RADIATION
UPPER LIMITS
PRESENT
EXPERIMENT
1/2 SOLAR
UPPER LIMIT
EXPECTED QUIET
SOLAR FLUX
COUNTS/CM²-SEC-keV
ENERGY (keV)
10⁻²
10⁻³
10⁻⁴
10⁻⁵
10⁻⁶
10⁻⁷
10
10²
10³
10⁴

FIG. 14

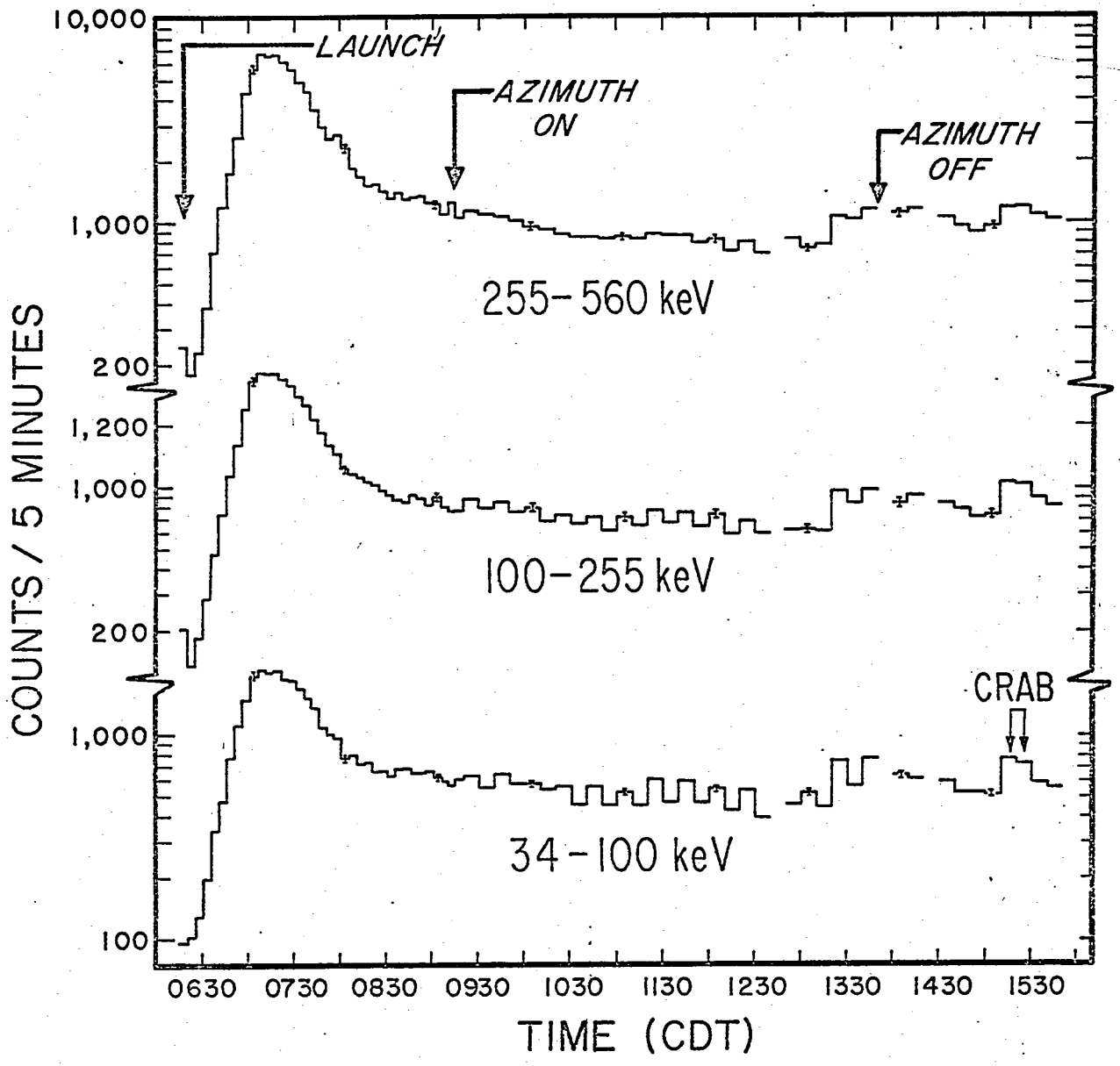
10,000
1,000
200
1,200
1,000
200
1,000
100
LAUNCH
AZIMUTH ON
AZIMUTH OFF
255-560 keV
100-255 keV
34-100 keV
CRAB
COUNTS / 5 MINUTES
0630
0730
0830
0930
1030
1130
1230
1330
1430
1530
TIME (CDT)

FIG. 15

around to view the Crab. At 1320 an increase is observed to commence in the background that is not correlated with any reported solar or geomagnetic activity. We have observed similar variations on other flights. The explanation for the variations is unknown, although Gregory and Kreplin (1967) have recently reported brief sporadic solar emissions of 1-10 keV x-radiation even when the sun is otherwise quiet; the background variations may be connected with this phenomenon.

An inspection of the ionization rate (Figure 13) shows no sudden increase at this time although it is in a period of general increase. This increase apparently is not connected with the gamma ray background jump since it can easily be explained as a latitude effect. The data of Neher (1967) show that at a constant altitude, in the region of 40° geomagnetic latitude, the ionization rate increases by approximately 6 ion pairs/sec-cm^3-atm. of STP air for each degree increase in latitude. Beginning about 1130 CDT the balloon began a Northward drift which resulted in a one degree change of latitude by 1430 CDT. The increased rate of ionization which was observed during this time is very consistent with this change.

From Figure 15 the general relation between background counting rate and altitude can be seen, but to account for such an increase, an altitude drop of approximately five thousand feet would be required in the space of five minutes. The altitude record shows no such violent altitude fluctuation.

Data from an earlier flight had been analyzed by Haymes and Craddock (1966) using the assumption that the background radiation was time-independent. Figure 15

shows that this assumption is invalid. Finally, the increase observed at about 1510 is due to a balloon rotation that caused the Crab and sun to pass once again into the field of view.

Figure 15a shows in more detail the portions of data used for determining the Crab Nebula's spectrum. The radiation due to the Crab was found by averaging the background segments which were adjacent in time to a Crab observation period, and then subtracting this average from the data obtained while the Crab was in the field of view. Thus a residual was formed for each Crab observation period. These residuals were then corrected for atmospheric absorption and for absorption due to the central photomultiplier, plastic scintillator and mounting hardware; this latter absorption correction was experimentally determined in the laboratory. It is shown in Figure 16. The curve was obtained by using various radioactive sources. The absorption is quite large (approximately a factor of four at 60 keV) at the lower energies and is even as large as 15% at 511 keV. Another model of the detector has been built that has a considerably smaller absorption factor.

The post-flight energy calibrations agree with those obtained prior to the flight; there is no evidence for any changes in the system during the flight. All portions of the data that contained any noise were discarded.

The Crab spectrum obtained by carrying out this procedure is shown in Figure 17. No portions of data were used beyond 1220, so that the spectrum is based upon 87 minutes of Crab observation and 94 minutes of background data. Radiation is observed at all energies within the range of the experiment, so that it is clear that gamma radiation has been detected from the Crab. The spectrum

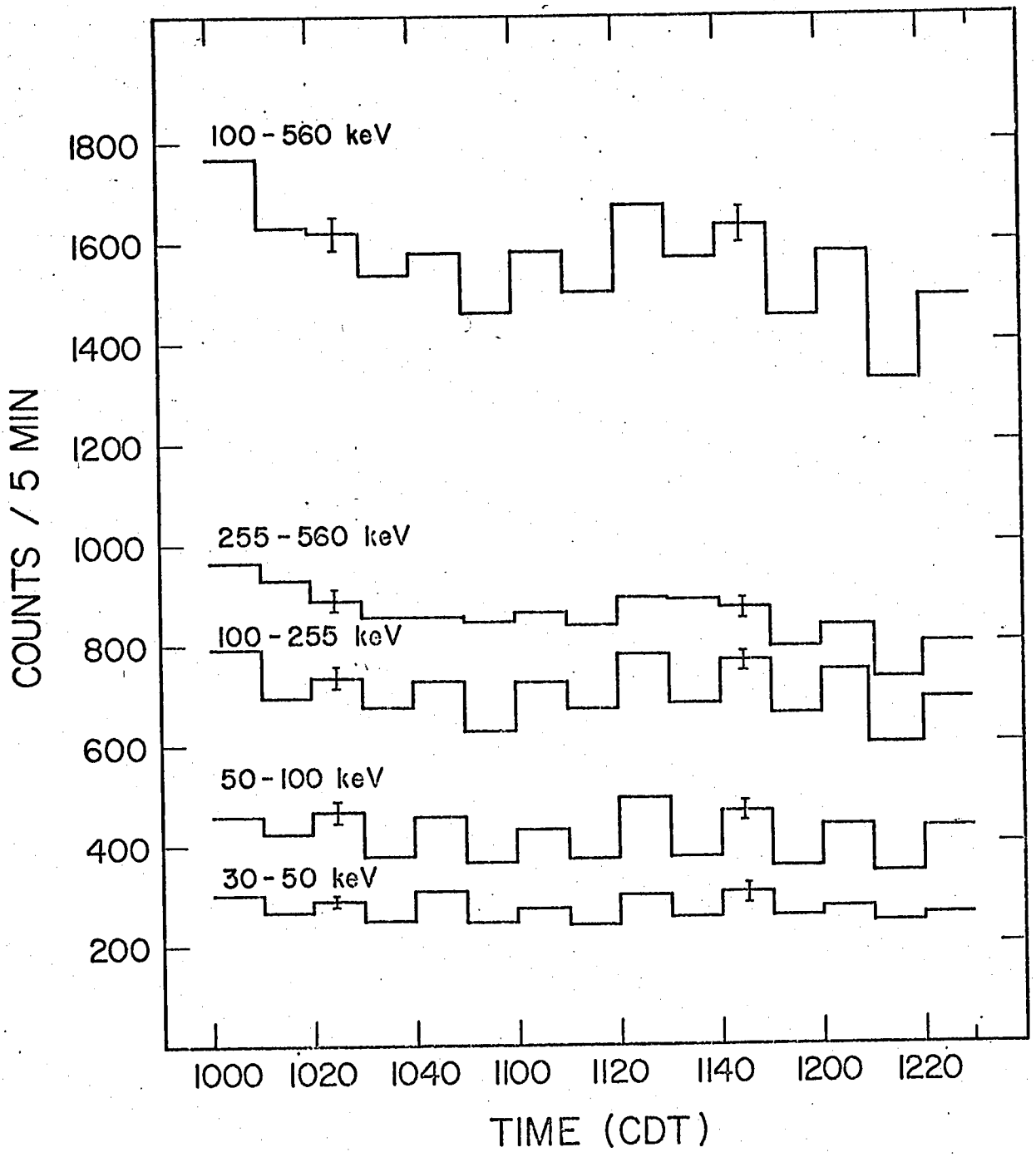
100 - 560 keV
255 - 560 keV
100 - 255 keV
50 - 100 keV
30 - 50 keV
COUNTS / 5 MIN
1800
1600
1400
1200
1000
800
600
400
200
1000
1020
1040
1100
1120
1140
1200
1220
TIME (CDT)

FIG. 15 a.

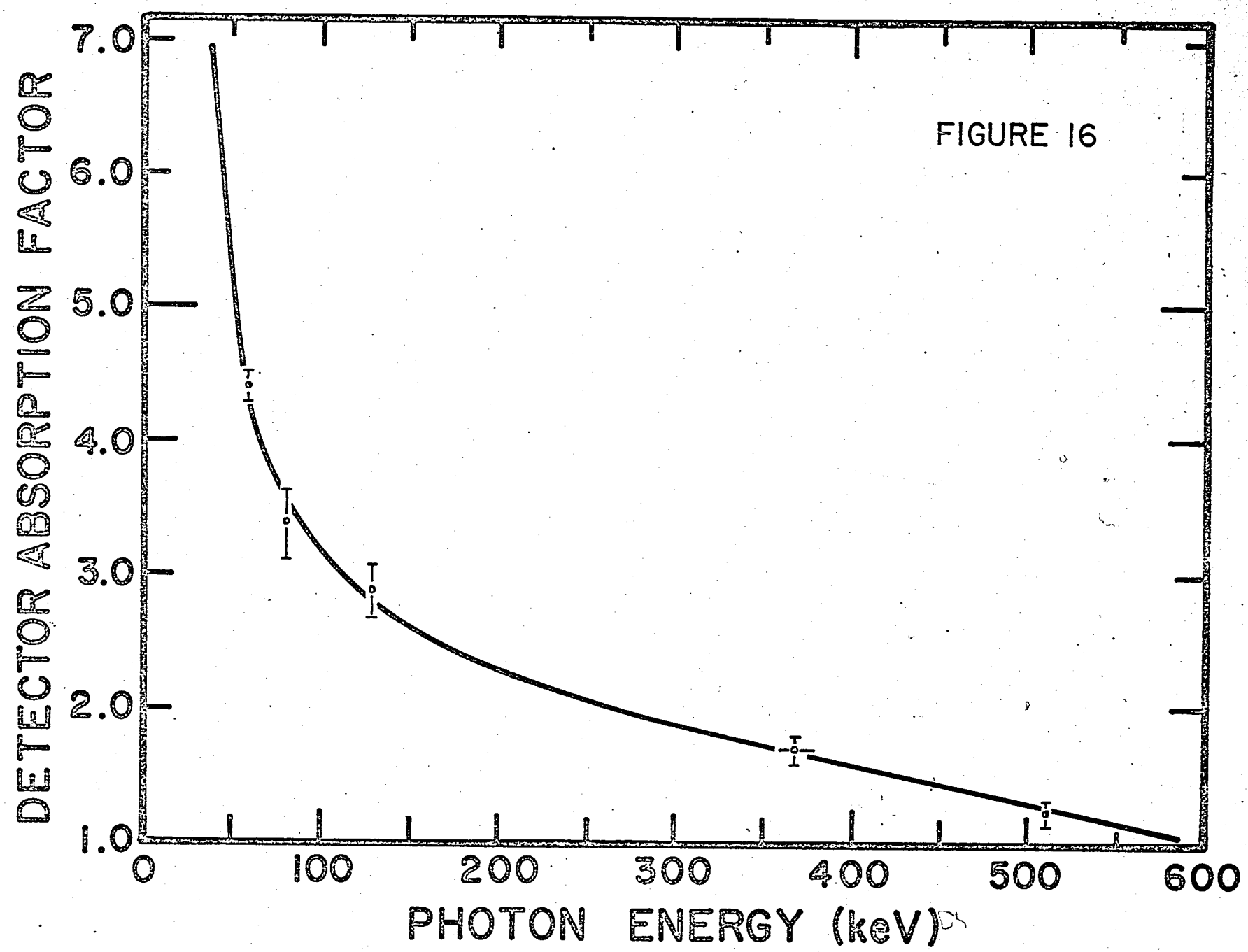
DETECTOR ABSORPTION FACTOR
7.0
6.0
5.0
4.0
3.0
2.0
1.0
0
100
200
300
400
500
600
PHOTON ENERGY (keV)

FIGURE 16

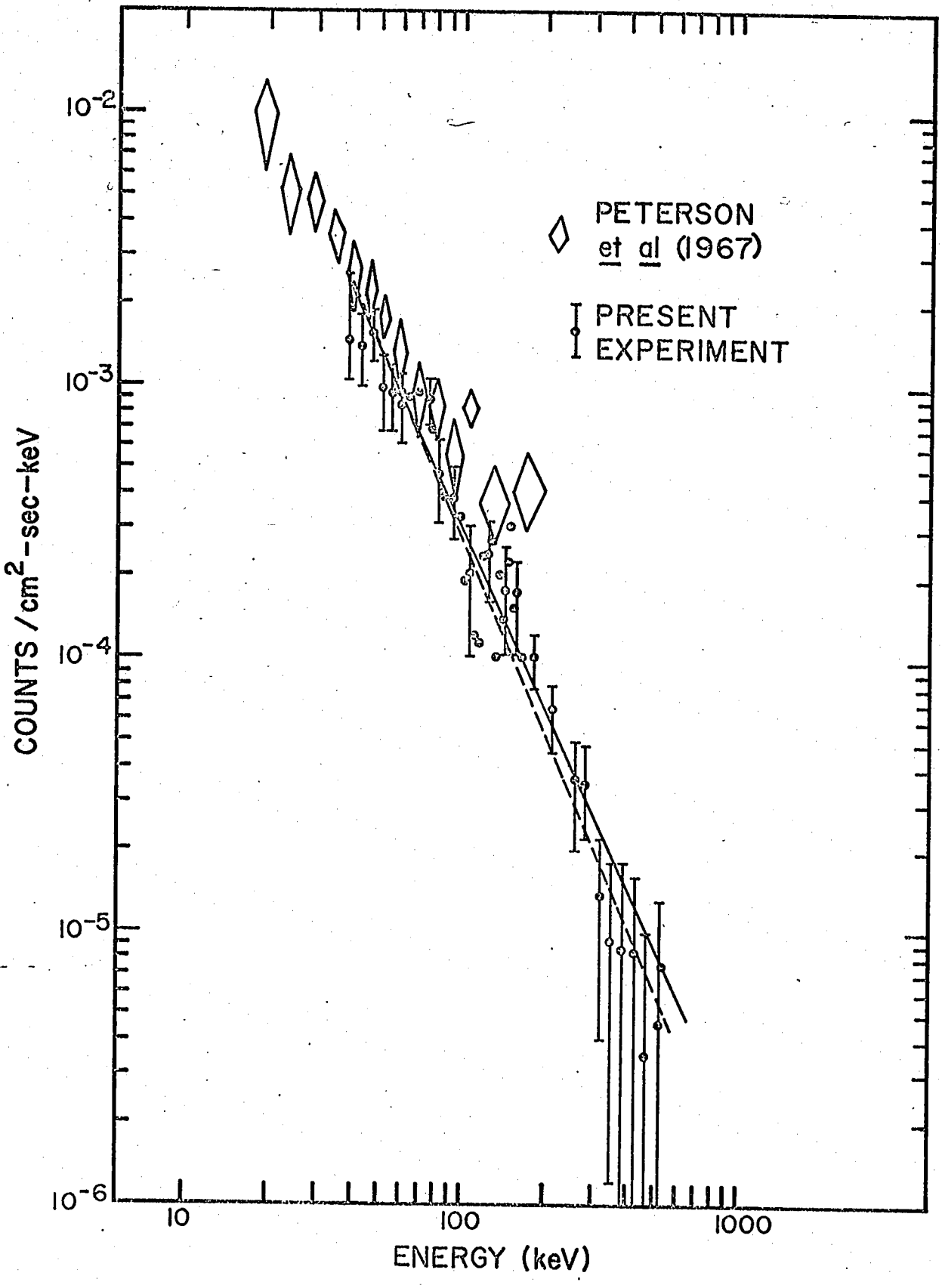
PETERSON
et al (1967)
PRESENT
EXPERIMENT
COUNTS /cm^2-sec-keV
10^{-2}
10^{-3}
10^{-4}
10^{-5}
10^{-6}
10
100
1000
ENERGY (keV)

FIG. 17

appears to be fit well by a power law. A least-squares fit to the data yields an expression of the form $dN/dE = (7.1 \pm 2.8)E^{-2.19 \pm .08}$ counts $cm^{-2}sec^{-1}keV^{-1}$. Therefore, the spectral index of the differential energy flux is $1.19 \pm .08$ over this range. The broad energy range covered in this experiment results in a very small standard deviation of the slope of the curve. The standard deviation is computed solely from the counting statistics; systematic error could introduce a larger uncertainty.

In the least-squares analysis, each data point was weighted in proportion to $1/\sigma^2$, where σ^2 is the variance of the point in question. If the data are not weighted, a spectral index of 1.37 results; this curve is shown as a dotted line in Figure 17. Subtraction of the upper limits for the sun found by Peterson et al. (1966) from our measurement also yields a power law, but with an index of approximately -1.4.

The above mentioned spectra can only be labeled as counting rate and not flux unless efficiency corrections are included in the data analysis. For NaI there are two effects to take into account. At the low energies (<200 keV) K-escape can occur. In this region of energies gamma rays are detected almost entirely by the photo-electric process. The ejection of a photoelectron from the K shell of an atom is followed by the emission of characteristic x-rays. If the interaction occurs near the surface of the crystal, Iodine K x-rays (28 keV) may escape without further interaction. In an ordinary scintillation crystal without anticoincidence circuitry this just produces another peak in the spectrum at 28 keV less than the photopeak, so that the photopeak efficiency

is lowered. However the escape of the K x-rays is followed by almost certain detection in the well crystal which then blocks the analyzer from registering the pulse from the central crystal, thus constituting a loss in the number of photons detected.

At higher energies (>200 keV) the cross section for absorption decreases, especially for the photoelectric interaction. Thus the peak efficiency begins to decline at these energies. This has been investigated for a 3 inch by 3 inch crystal by Neiler and Bell (1965).

Figure 18 shows the correction factor to transform our measured counting rate into absolute flux. The data for the K x-ray escape correction are given by Axel (1954). When these corrections are applied to the measured spectrum of the Crab the spectral slope is reduced by approximately 0.1. Thus we conclude that the corrections are relatively unimportant. This appears to be contrary to the conclusion of Stein and Lewin (1967) who expect that reanalysis of their data, taking escape corrections into account, might lead to considerably different conclusion as to the form of the incident spectrum. Those investigations, however, considered only low-energy spectra; our data are taken over a much broader range of energies.

Shown also in Figure 17 are the results of Peterson et al. (1967) which match our fluxes reasonably well in the region of overlap, although the spectrum we have found for the x- and gamma radiation from the Crab is steeper than the spectrum that best fits the data points obtained by those investigators for the hard x-radiation alone. The dependence on energy found here seems to be in somewhat better agreement with the index of 1.3 ± 0.2 obtained by

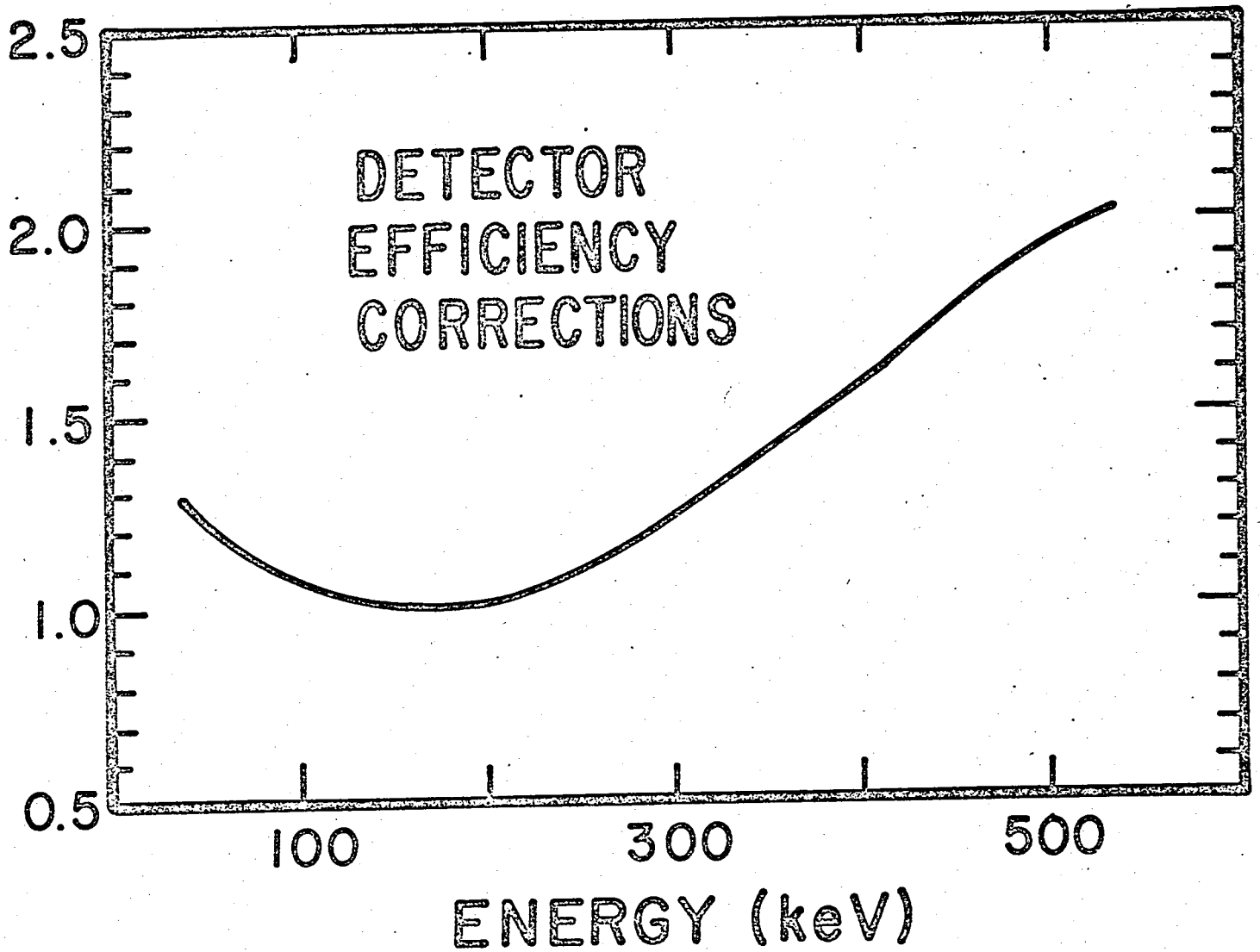
2.5
2.0
1.5
1.0
0.5
DETECTOR
EFFICIENCY
CORRECTIONS
100
300
500
ENERGY (keV)

FIG. 18

Grader et al. (1966) for the soft x-ray spectrum; it also fits more smoothly to an extrapolation of the optical spectrum.

The pulse height analyzer was arranged so that all photons with energies in excess of 560 keV were included in one integral channel. The upper limit on this "overflow" counting rate is 2.4×10^{-3} $cm^{-2}sec^{-1}$, with a 95% confidence. No statistically significant deviations from this power law fit to the continuum spectrum were observed.

Since only a continuum was apparent, upper limits can be placed at the energies of the three strongest line emissions that were predicted for the Crab by Clayton and Craddock (1965), on the basis of the Californium hypothesis. In addition to these we have also placed an upper limit on the 511 keV line that might be expected from positron annihilation. These results, at the 95% confidence level, are shown in Table III where we have assumed the absolute efficiency of the central crystal to be like that of a 3 inch by 3 inch detector (Neiler and Bell, 1965).

TABLE III

Energy (keV)	Clayton and Craddock Estimate ($cm^{-2}sec^{-1}$)	Upper Limit ($cm^{-2}sec^{-1}$)
60	5.7×10^{-5}	3.9×10^{-3}
180	1.0×10^{-4}	1.5×10^{-3}
390	9.7×10^{-5}	9.5×10^{-4}
511	----------	8.4×10^{-4}

These upper limits are considerably below the fluxes calculated earlier by Savedoff (1959), who assumed that $10^{-2} M_{\odot}$ of Cf^{254} were formed during the explosion.

No time variations greater than about 46% in the flux with characteristic times of 1-1/2 year are apparent, at least up to energies of the order of 120 keV. This is the highest energy radiation previously detected from the Crab (Peterson et al., 1967) and is therefore the highest energy data with which we may compare our results.

In Figure 22 we present a summary of data on the spectrum of the electromagnetic radiation from the Crab Nebula. It appears that the gamma-ray spectrum matches well with the results of rocket-borne experiments of others (Grader et al., 1966), that have explored the soft x-ray spectrum down to energies of about 2 keV. Thus the whole x-and gamma-ray region may be characterized by the same spectral index.

IV. Discussion

A. Detectability of Gamma-ray Line Emission from the Crab

In the paper by Clayton and Craddock (1965) the possibility of observing gamma rays from the Crab Nebula was discussed in connection with estimates of background to be expected at balloon altitudes. In light of our new measurements the situation must be reviewed.

Figure 19 shows the spectrum calculated by Clayton and Craddock as "seen" by our detector. To produce the line shapes the resolution was taken to be 8.9% as measured at 662 keV in the laboratory and with the analyzer gain set to be 4.25 keV/channel. The detected lines were taken to be purely of Gaussian shape with no Compton "shelf" taken into account' this latter effect would make the peaks somewhat harder to see. The line shape is then of the form

$$N(x) = N_o \exp(- (x-x_o)^2/b_o) ,$$

where $N(x)$ is the counting rate in channel number x, x_o is the photopeak position, and the resolution (FWHM), r, is given by

$$r = \frac{2\sqrt{\log_e 2}\ \sqrt{b_o}}{x_o} .$$

Since the resolution varies as the inverse square root of the incident photon energy, for a normalized line flux the number of counts in the peak channel varies with the energy of the incident flux. In Figure 20 the ratio

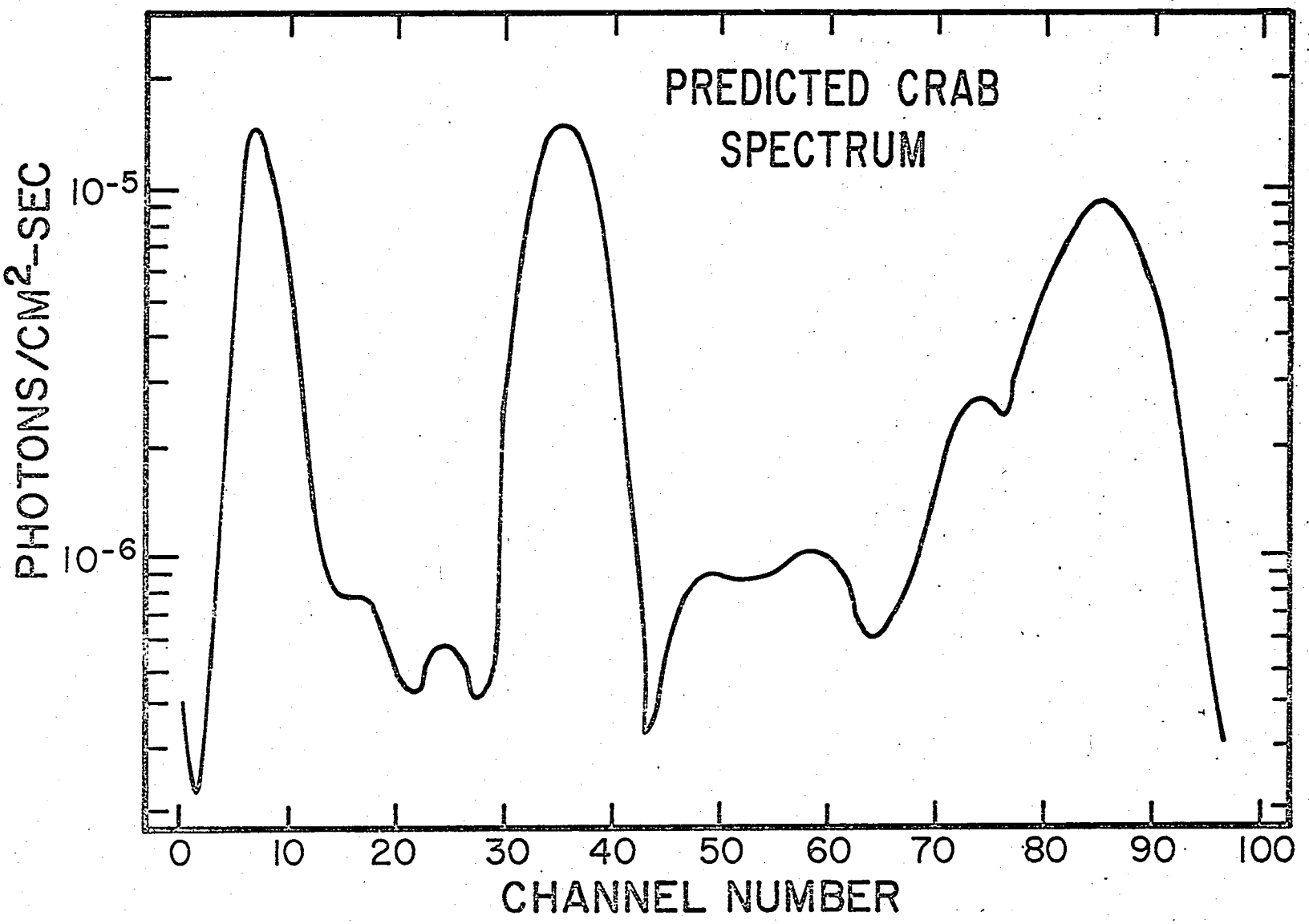
PREDICTED CRAB
SPECTRUM
PHOTONS/CM^2-SEC
10^{-5}
10^{-6}
0
10
20
30
40
50
60
70
80
90
100
CHANNEL NUMBER

FIG. 19

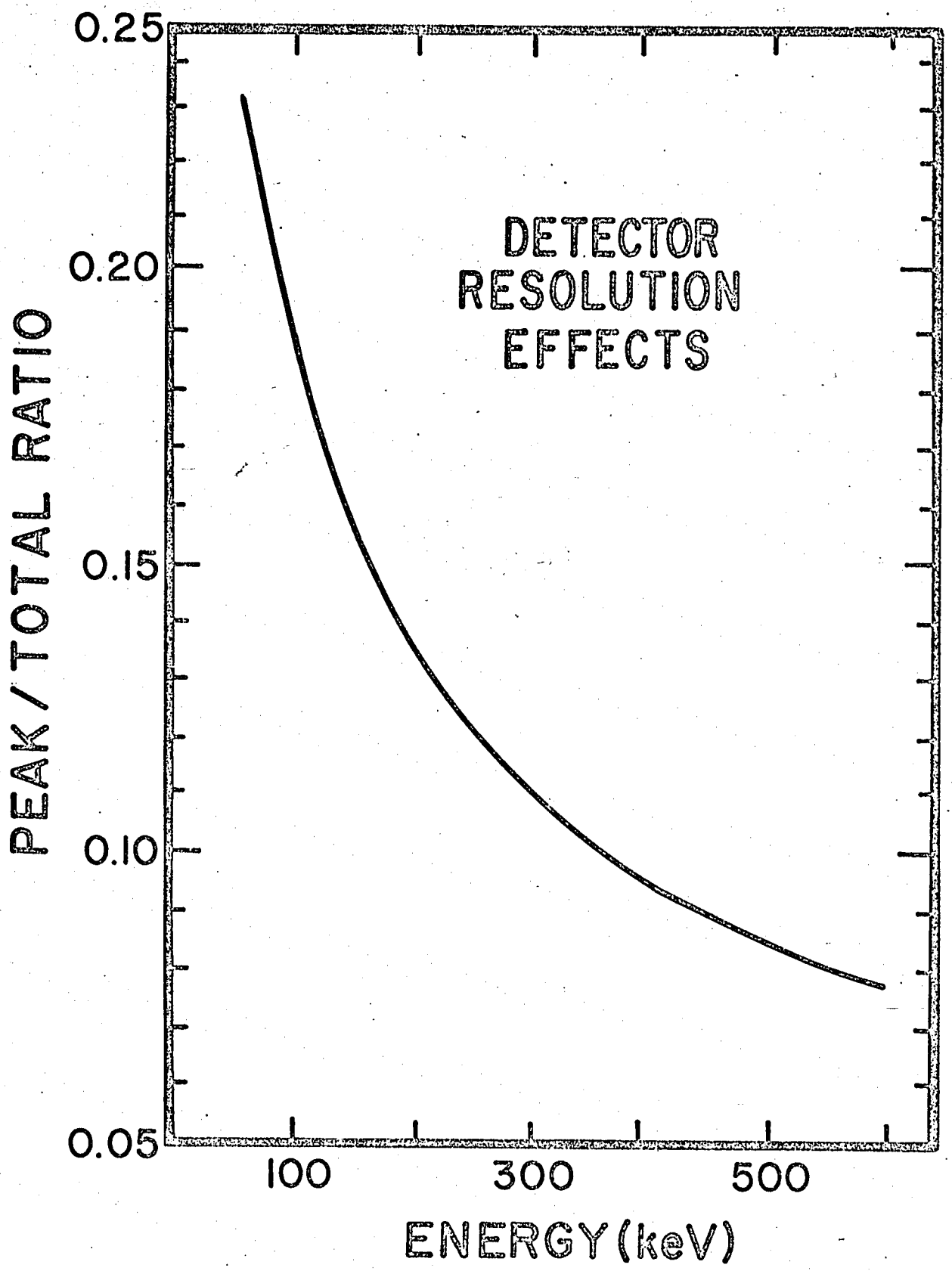
0.25
0.20
0.15
0.10
0.05
PEAK / TOTAL RATIO
DETECTOR
RESOLUTION
EFFECTS
100
300
500
ENERGY (keV)

FIG. 20

of the peak channel counting rate to the total line flux is plotted versus the energy of the incident flux for the resolution of our detector.

In Figure 21 our measurement of the Crab's spectrum is presented with the histograms representing the additional predicted flux from the Crab superimposed on this continuum. This demonstrates the difficulty of detecting a small flux. It is not just the atmospheric background problem (since this has already been subtracted out) but the real problem lies with the natural background or continuum associated with the Crab. This continuum is so bright that it swamps any expected line contribution.

At 180 keV the ratio of line flux to continuum is 15% and at 390 keV the ratio is 40% at the peak positions. With the present detector system this is not detectable since the standard deviations at these channel numbers were 20% and 90% respectively, of the total counts detected. At least an excess of two or three standard deviations is required for positive identification.

This matter can be improved in a number of ways. Obviously nothing can be done to remove the continuum of the Crab; this type of "background" is unavoidable. However, by increasing the resolution significantly (by means of an efficient solid-state detector) the peak counting rates will be more easily identifiable.

Other improvements can deal with reducing the size of the relative standard deviations of the data. This can be done in several different ways.

The first is to increase the total number of counts. This can be done either by increasing the size of the

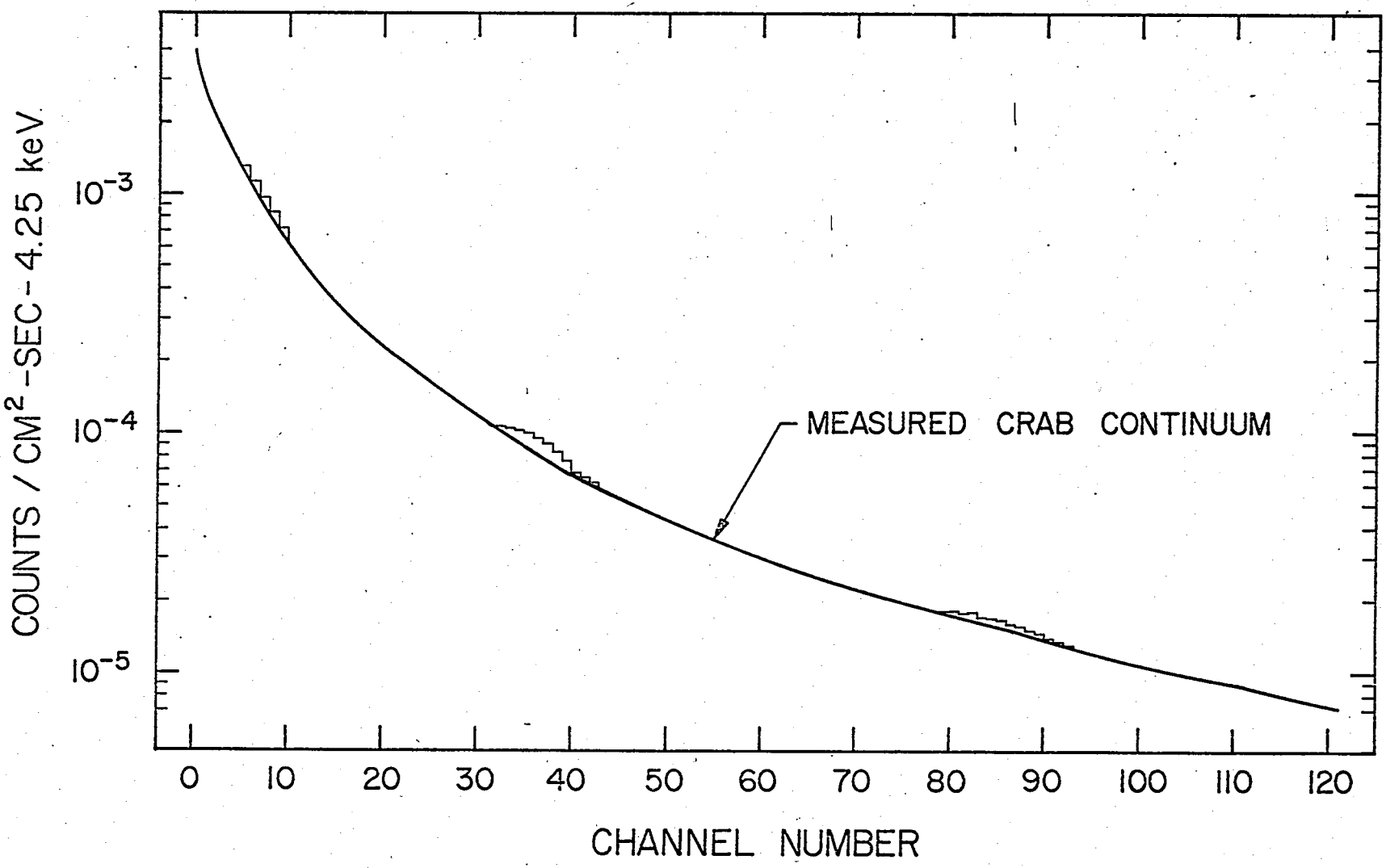
COUNTS / CM^2-SEC-4.25 keV
10^{-3}
10^{-4}
10^{-5}
MEASURED CRAB CONTINUUM
0
10
20
30
40
50
60
70
80
90
100
110
120
CHANNEL NUMBER

FIG.21

detector area or increasing the observation time. If the area of the detector is increased the shielding requirements also increase and become economically unfeasible when dealing with a NaI collimator. To increase the observation time in a balloon experiment is very difficult. If the object is tracked for ±3 hours from transit one only obtains three hours of observation time because half of the six hours must be spent in obtaining background data. Increasing the observation to times where the zenith angle is greater than 45^{o} is fruitless because of the increasing path length through the residual atmosphere. Consequently to gain a factor of ten or so in the observing time, a balloon experiment is not feasible. The advent of precisely oriented satellites may provide the optimum vehicle from which to perform this experiment.

Another way of improving the statistics is to decrease the background rate. This can be done perhaps, with increased shielding and narrowing down the solid angle of observation, and by preventing neutron activation in the NaI detector. A new detector system is presently being designed that will take these shielding requirements into the design criteria.

B. Luminosity of the Crab

In Figure 22 a summary of data on the spectrum of the Crab Nebula is presented. The data on the radio region are compiled in Howard and Maran (1965) and the infrared data are from Morroz (1964), Kleinman (1967), and Becklin (1967). The observations in the visible have been made by O'Dell (1962). There is, however,

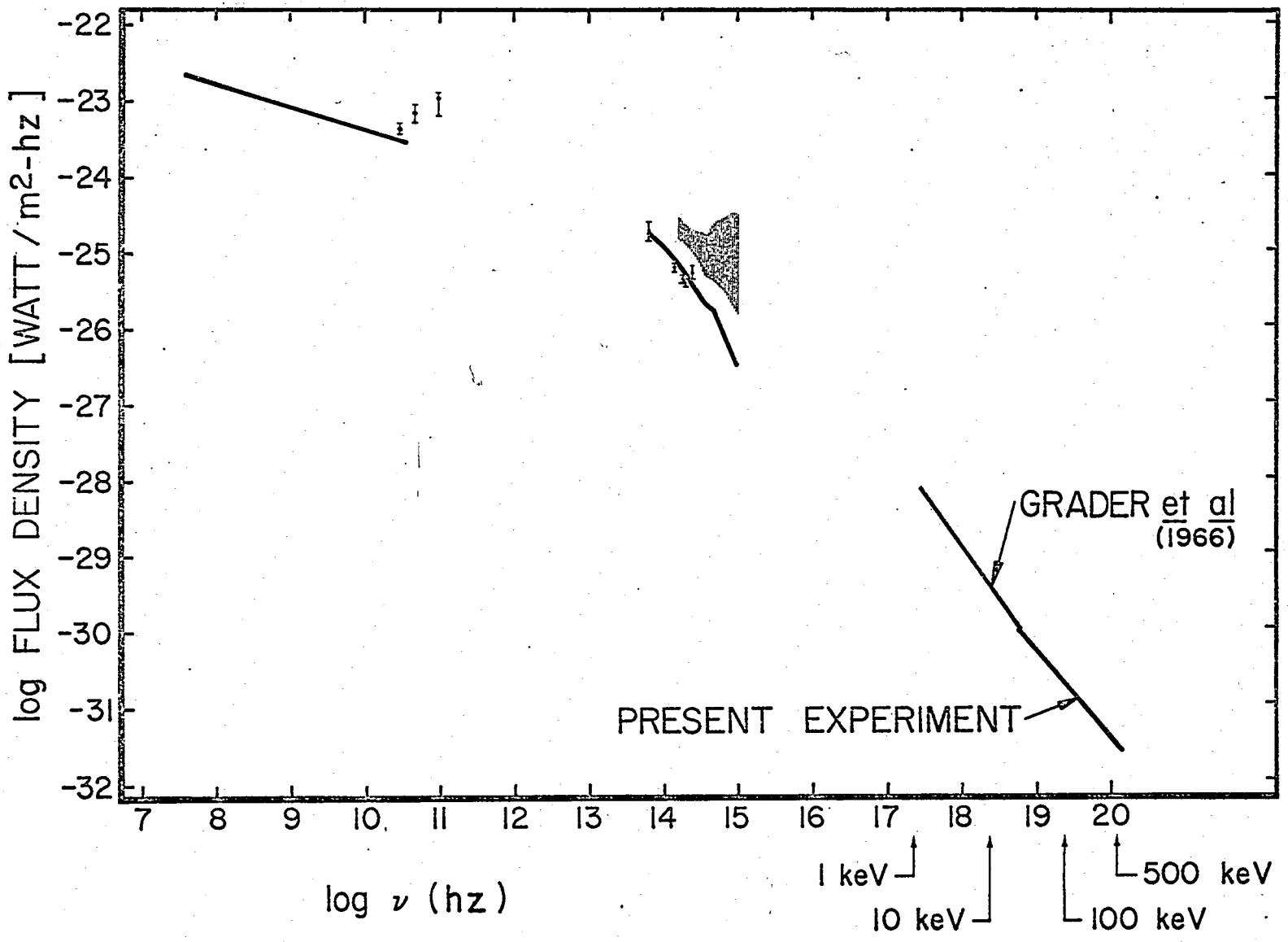
log FLUX DENSITY [WATT / m2-hz]
-22
-23
-24
-25
-26
-27
-28
-29
-30
-31
-32
7
8
9
10
11
12
13
14
15
16
17
18
19
20
log ν (hz)
GRADER et al
(1966)
PRESENT EXPERIMENT
1 keV
10 keV
100 keV
500 keV

FIG. 22

some uncertainty over the size of the correction for interstellar absorption to be used. The shaded block represents the possibilities of the spectral shape if the absorption is between $1^m.1$ and $3^m.2$, the former having been considered the most reasonable by O'Dell. It could, however, be as small as $0^m.7$ (Morroz, 1964). Three measurements in addition to the present experiment have been presented for comparison in the x-ray region.

It appears that the power radiated in the x- and gamma ray radiation is a power law varying as $1/E^{1.2}$. This type of spectrum appears to join smoothly with O'Dell's optical measurements when corrected for $A_v = 1^m.6$.

From the many observations of the Crab over the spectrum from 10^8 to 10^{19} Hz it is possible to construct an idealized spectrum with a break occurring at $\sim 10^{14}$ Hz. In this case the spectral index is 0.3 between 10^8 and 10^{14} Hz, and 1.2 for frequencies between 10^{14} and 10^{19} Hz. The general form of the spectrum can be written as

$$J = A\nu^{-\alpha} ,$$

where α, is the spectral index and the constant of proportionallity can be determined from two points lying on the two different portions of the spectrum.

For a spectrum of this type a luminosity can be defined by

$$L = 4\pi R^2 \int_\nu A\nu^{-\alpha} d\nu$$

$$= 4\pi R^2 \frac{A}{1-\alpha}(\nu^{1-\alpha}) \text{ erg/sec},$$

where R is the distance to the source.

Using a distance of 1030 pc to the Crab, the

luminosity is found to be 1.3×10^{37} erg/sec and if the distance is 1700 pc as suggested by Shklovskii (1966), and Scargle (1967) the luminosity becomes approximately 3.5×10^{37} erg/sec. This is an order of magnitude larger than previously calculated (Burbidge, 1966).

The radioactive input was estimated to be only 1.2×10^{36} erg/sec (Clayton and Craddock, 1965) and from our measurements of the upper limits on the radioactive level the energy input by this means certainly cannot be much larger than a factor of ten times this figure. The predicted radioactivity energy input to the present-day energy balance cannot be more than about 4% of the total required!

As Shklovskii (1966) has pointed out, the distance to the Crab is most likely 1700 pc as opposed to the earlier value of 1030 pc. Since the increase in the distance to the Crab requires an increase in the amount of interstellar absorption Shklovskii estimates this to be $A_v = 1^m.6$ and then quotes the optical spectral index to be 0.80. However from the tables listed in O'Dell (1962), it can be determined that the slope or spectral index is more nearly 1.2.

An extrapolation of our gamma-ray measurement into the optical region gives good agreement with a correction of $1^m.6$. In addition if one extends this extrapolation to radio frequencies and uses the somewhat curious measurements of Tolbert (1965) in the millimeter range, a maximum is caused to occur in the spectrum at about 10^{12} Hz. This maximum could be expected as a natural consequence of continuous injection of relativistic electrons into the Crab. That relativistic electrons are continuously being injected into the Crab is almost certain as pointed out by Tucker (1967). From this some-

what uncertain maximum Shklovskii was able to determine that the average magnetic field should be approximately 7×10^{-4} gauss.

C. Gamma-Ray Emission Mechanisms

Observations and theoretical arguments have led to two generally accepted source mechanisms for the plasmas in discrete x- and gamma ray sources. The two most feasible are bremsstrahlung and synchrotron radiation from a high temperature low density gas. Neutron stars are no longer considered as a source because of their rapid cooling rates and the lack of observational evidence of a black body spectrum.

It should be pointed out that the determination of the source mechanism from the spectral shape is a difficult task and in past review articles this fact has not been emphasized. In actuality neither of the two proposed source mechanisms gives rise to a unique spectral shape. A synchrotron source has a power-law spectrum only if the distribution of the relativistic electrons follows a power-law. Thermal bremsstrahlung gives rise to a simple exponential only if the entire plasma is at one temperature. Thus if there are any temperature gradients a variety of shapes can exist as has been pointed out by Sartori and Morrison (1967). Manley (1966) has shown that a sharp cut-off in a flat electron spectrum will result in a synchrotron spectrum of an approximately exponential shape.

1. Thermal Bremsstrahlung

A hot, optically thin plasma of temperature T is efficient for the production of keV type x-rays. In this

case the spectrum has a unique shape and is given by:

$$J(E)dE = \text{Const. } \exp(-E/kT)dE \quad ,$$

where $J(E)dE$ is the energy flux of x-rays between E and E+dE. Consequently the number spectrum is given by:

$$N(E)dE = 1/E \text{ Const. } \exp(-E/dT)dE \quad .$$

On the basis of their recent measurements of the Crab, Clark et al. (1967) are unable to decide on the spectral shape. Their measurement between 11 keV and 70 keV fits an exponential and power law equally well. For this experimental curve, the values of kT between 40 and 80 keV are consistent while the power law exponent ranges from -1.8 to -1.4. Peterson et al. (1967) state that their previous fit (Peterson, Jacobsen, and Pelling, 1966) of $E^{-1.91}$ is still an adequate representation of their more recent data.

The wide energy range of our measurement, on the other hand, provides a very good determination of the spectral shape and we have found it to be of the form of a power law. A single exponential definitely is not consistent with our measurements.

Still the "hot-gas" model for x-ray sources is popular. Sartori and Morrison (1967) have argued that a hot gas is produced any time electrons are accelerated. They ascribe the x-ray spectrum of the Crab to a bremsstrahlung source with important contributions from plasmas at two distinct temperatures; kT near 2 keV and near 40 keV. Such a distribution produces the spectrum shown in

Figure 23. It is indeed similar to a power-law over a limited range and fits Peterson's data and the rocket-based data well. However beyond 100 keV it drops off sharply and is not consistent with the rest of the spectrum that we have measured.

No reason was given for expecting two temperature distributions but it seems apparent that one can construct a power-law spectrum out of a large number of thermal sources. Whether it is reasonable to do so may be questionable.

As a possible explanation of x-ray sources it might be worthwhile to consider what type of spectrum is produced by a plasma possessing a continuous temperature distribution rather than to expect it to be of a uniform temperature. To expect an object of the dimensions of the Crab to have a uniform temperature distribution seems unreasonable.

To derive the temperature distribution which produces a power-law photon spectrum we require

$$\sum_{T} n(T) \frac{1}{\sqrt{KT}} \exp(-E/KT) = AE^{-\gamma} \quad ,$$

where n(T) is the number of electrons at a given temperature. The above equation was required to be valid for photon energies between 30 and 500 keV.

The easiest approach to this problem was the formation of N simultaneous equations of the above form for N values of E between the specified limits. Various values of temperature T, were chosen up to as many as 50 in a given set. The resulting array of simultaneous equations was solved by a computer. The surprising result was that

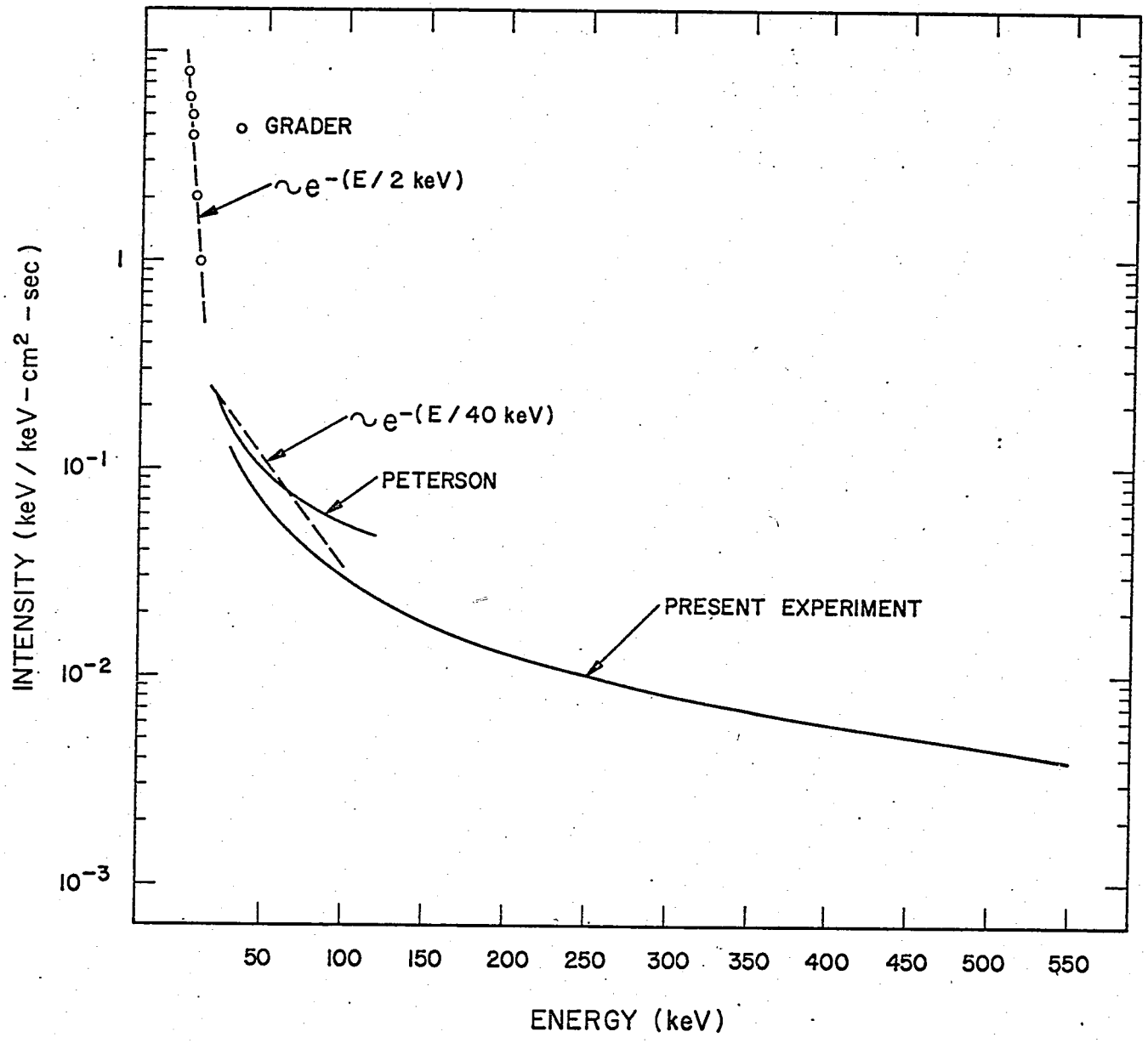
o GRADER
~e^-(E/2 keV)
~e^-(E/40 keV)
PETERSON
PRESENT EXPERIMENT
INTENSITY (keV / keV-cm² - sec)
1
10^-1
10^-2
10^-3
50
100
150
200
250
300
350
400
450
500
550
ENERGY (keV)

FIG. 23

for all cases considered the function n(T) was not smooth or continuous and usually half of its computed values were negative. This is clearly non-physical. Thus it is concluded that no physical temperature distribution is capable of producing the power-law spectrum as measured for the Crab via thermal bremsstrahlung in this energy range.

2. Synchrotron Radiation

For some years now the radiation from the Crab Nebula in the optical and radio region has been known to be due to the synchrotron process. This hypothesis was first confirmed by Oort and Walraven (1956) with the measurement of polarized light from the Crab.

Because the radio observations obey a power-law distribution one can deduce from the theory of synchrotron emission that a power-law distribution of electrons is required to account for this radiation. However the synchrotron hypothesis predicts a continuous distribution of flux over all energies with the same spectral index. As can be seen there is an apparent break in the spectrum at approximately 10^{14} Hz. This can be explained in a simple way on the basis of the synchrotron hypothesis. If the initial electron distribution in the Crab was power-law, then due to synchrotron radiative losses, the higher energy electrons are transformed in time to lower energy electrons and the whole distribution function translates to lower energies. In addition to this translation there is an additional break which develops in the spectrum of electrons because of the critical dependence of radiative lifetime on electron energy. Thus the break in the synchrotron spectrum is a reflection of the break which

develops in the electron spectrum. If one assumes no injection of relativistic electrons from the synchrotron loss formula it is possible to predict the ratio of the spectral indices of the two portions of the spectrum. This is found to be $\frac{3}{2}\frac{(\gamma-1)}{(2\gamma+1)}$ (Kardashev, 1962), where γ is the exponent appearing in the electron distribution. From the radio measurements γ is found to be 1.6 so the slope of the x-ray region should be 1.4, but the measurements show the index to be about 1.2.

This discrepancy could have been anticipated on the basis of a lifetime argument (Gould and Burbidge, 1965), which predicts no energetic electrons of sufficient energy to produce gamma rays to be present some 900 years after the initial explosion. However there is the possibility that there was injection of relativistic electrons up until a few years ago.

Another view which might be taken of the Crab is that the radio-optical branch might be unrelated to the x- and gamma ray portion of the spectrum. Thus the radio portion can be adequately explained on the basis of synchrotron emission of an initial spectrum of electrons injected 900 years ago. Then the explanation of the x- and gamma ray branch is open to discussion. However one is led back to considering the suggestion of Sartori and Morrison (1967) which predicts a radio spectrum produced by relativistic electrons and the secondary production of a hot gas which then can account for the x-ray emission.

As a possible mechanism for providing relativistic electrons it might be worthwhile to revaluate the so-called "light-ripples" which have been observed in the Crab. These are thought to be hydro-magnetic waves and supposedly can contain up to 10^{44} ergs (Woltjer, 1957).

If the electron spectrum is integrated out to 2×10^{14} eV the total electron energy injected into the Crab in the form of relativistic electrons is about 5×10^{49} ergs or about 30 times greater than previously estimated (Gould and Burbidge, 1965).

V. Conclusion

It is clear that the Crab Nebula does indeed emit gamma rays. A continuum spectrum has been observed. The most likely explanation for this radiation is the synchrotron process. Temperature of the order of 5×10^9 ^oK would be required to produce the observed 500 keV radiation by means of thermal bremsstrahlung.

A. Line Gamma Emission

The emission of gamma-rays by the Crab Nebula due to radioactivity cannot be ruled out on the basis of this measurement. But the amount of radioactivity predicted has now been shown to be a minor contribution to the present-day energy balance. On the basis of the Californium-hypothesis, radioactivity can account for only about 4% of the integrated luminosity.

Moreover this measurement contradicts the proposal of Morrison and Sartori (1965) which attributes the Crab x-ray source to thermal bremsstrahlung from a hot plasma of a high-Z material requiring continuous heating by unspecified radioactive isotopes. The measured power-law spectrum precludes this thermal model.

B. The Continuous Spectrum

As a result of this experiment the continuum is now known to extend to at least 560 keV. From this measurement, the x-ray and gamma-ray portion of the Crab Nebula's spectrum appears to be part of a unified synchrotron spectrum for this object. The observed 560 keV radiation implies that electrons with energies up to 2×10^{14} eV are present,

if the Crab's magnetic field is 2×10^{-4} gauss. This field strength is estimated from the observed break in the optical region of the electromagnetic spectrum. The gyro radius of such an electron is 3×10^{15} cm, some 5 times the mean radius of Pluto's orbit about the sun.

The magnitude and slope of the gamma-ray spectrum allow it to be joined smoothly with optical data corrected to an absorption of $A_v = 1^m.6$ which now appears to be a reasonable interstellar correction (Shklovskii, 1966).

A further verification that the x-ray and gamma-ray portion of the Crab's spectrum is due to synchrotron radiation could be made by a polarization measurement which has been suggested by Dolan (1966). In his report the degree of polarization is expected to be about 50% at 3 Å. However by the method he proposes, a 100 cm^2 detector would require approximately 14 hours observing time to determine the degree of polarization of the Crab.

An additional investigation should be made of the apparent change in sign of the spectral index of the radio data at 10^{11} Hz. Also, if a maximum does indeed exist around 10^{14} Hz a better determination of the average magnetic field in the Crab can be made and the continuous injection of relativistic electrons will be confirmed.

Finally, the discovery of gamma radiation from a celestial source, as described in this thesis, has created more problems than it has solved in our understanding of high-energy cosmic events. It is to be hoped, however, that additional observations in this wavelength region will bring some order to the present rather chaotic situation.

APPENDIX I.

Data Analysis-Curve Fitting

Nuclear gamma rays occur as random events and therefore follow the Poisson statistical distribution. However, the Gauss distribution is often used because it describes the distribution of random errors in many kinds of measurements (Young, 1962). It is more practical to accept the Gauss distribution whenever the number of events is large; this distribution is frequently called the "normal distribution".

Consider the probability of occurrence of the set of measurements y_i where the measurements are normally distributed according to the Gauss distribution. The probability of obtaining a measurement within dy of y_i is given by

$$P_i = \frac{1}{\sigma\sqrt{2\pi}} e^{-(y-y_i)^2/2\sigma_i^2} dy,$$

where σ_i is the standard deviation of y_i. The probability of obtaining the whole set of N measurements is the product of the separate probabilities:

$$\begin{aligned} P &= P_1 P_2 \cdot \cdot \cdot P_N \\ &= \left(\frac{1}{\sigma\sqrt{2\pi}} e^{-(y-y_1)^2/2\sigma_1^2} dy\right) \cdot \cdot \cdot \left(\frac{1}{\sigma\sqrt{2\pi}} e^{-(y-y_N)^2/2\sigma} \right. \\ &= \left(\frac{dy}{\sigma\sqrt{2\pi}}\right)^N \exp\left(\frac{1}{2}\sum_{i=1}^{N} (y-yi)^2/2\sigma_i^2\right) . \end{aligned}$$

The principle of least squares has its foundation in the above equation. To maximize the probability, P, one must

minimize the sum

$$M = \sum_{i=1}^{N} \frac{[y-y(x_i, a_\lambda)]^2}{\sigma_i^2} \quad ,$$

where a_λ are parameters upon which the data depends. This is done by solving the simultaneous equations

$$\partial M/\partial a_\lambda = 0. \qquad \lambda = 1 \rightarrow \nu.$$

To find the standard deviation of the parameters, a_λ, the error matrix $H_{\lambda\mu}$ must be calculated. Its elements are given by $H_{\lambda\mu} = \frac{1}{2}\partial^2 M/\partial a_\lambda \partial a_\mu$. The standard deviations of the parameters are given by the square roots of the diagonal elements of the inverse matrix H^{-1}, so that $\sigma_a = \sqrt{(H^{-1})_{aa}}$ etc. (Melissinos, 1966).

As a special application of the method of least squares we have worked out the details for the general fitting of a curve to a power law where the standard deviation, σ_i, is known for each data point. There is not much published literature that explicitly portrays the least-squares analysis for anything more complicated than a linear relationship. In general most methods assume σ_i's to all be equal but in our case this was not true. We incorporated the variation of σ into the determination of the best fit.

In this case the set of N measurements is the counting rate C_i; these are related to the energy E, by the theoretical relationship $C_i = A\ E_i^{-\gamma}$, where A and γ are positive constants.

Consequently the sum to minimize is;

$$M = \sum_{i=1}^{N} \frac{(C_i - A\,E_i^{-\gamma})^2}{\sigma_i^2} \tag{1}$$

The conditions for a minimum are;

$$\partial M/\partial A = 0 = -2 \sum_{N} 1/\sigma_i^2 (C_i - A\,E_i^{-\gamma}) E_i^{-\gamma} \tag{2}$$

$$\partial M/\partial \gamma = 0 = 2 \sum_{N} 1/\sigma_i^2 (C_i - A\,E_i^{-\gamma}) A\,E_i^{-\gamma} \ell n E_i \tag{3}$$

From eq. 2 we find

$$A = \frac{\sum_{N} 1/\sigma_i^2 C_i E_i^{-\gamma}}{\sum_{N} 1/\sigma_i^2 E_i^{-\gamma}} \tag{4}$$

and this is substituted into eq. 3 to yield

$$\sum_{N} 1/\sigma_i^2 (C_i E_i^{-\gamma} \ell n E_i) - \left(\frac{\sum_{N} 1/\sigma_i^2 C_i E_i^{-\gamma}}{\sum_{N} 1/\sigma_i^2 E_i^{-2\gamma}} \right) \sum 1/\sigma_i^2 (E_i^{-2\gamma} \ell n E_i = 0 \tag{5}$$

Since this equation is nonlinear and since we are dealing with the case of N = 127 the problem is best handled by a computer. A program (see Table IV) was written to solve eq. 5 by successive approximation; this program is for use with the IBM 1620 digital computer. The value of γ was varied until the expression in eq. 5 was very nearly ($\sim \pm 10^{-8}$) equal to zero. Then using the appropriate value of γ, A was found from eq. 4 and thus they represented the best values of parameters to minimize the sum in eq. 1.

TABLE IV

```
C       POWER-LAW LEAST SQUARES FIT
        DIMENSION E(126),C(126),SIGSQ(126)
        READ1,N
      1 FORMAT (I5)
        READ3,GAM
        DO2 I=1,N
        READ3,E(I),X,SIG
        C(I)=X
      2 SIGSQ(I)=SIG**2.
      3 FORMAT(3E20.5)
        PUNCH40
     40 FORMAT(35HFLIGHT 67-1      86 MINUTES OF CRAB)
        PUNCH 6
      6 FORMAT(33HGAMMA    INTERCEPT    MINIMIZED SUM)
        TEST=0.
        DEC=.05
     10 SUMT=0.
        SUMB=0.
        SUMX=0.
        SUMY=0.
        DO4 I=1,N
        EGAM=1./E(I)**GAM
        ELE=LOG(E(I))
        T=C(I)*EGAM/SIGSQ(I)
        B=T*EGAM/C(I)
        X=T*ELE
        Y=B*ELE
        SUMT=SUMT+T
        SUMB=SUMB+B
        SUMX=SUMX+X
      4 SUMY=SUMY+Y
      5 CONTINUE
        A=SUMT/SUMB
        Z=SUMX-(SUMT/SUMB)*SUMY
        PUNCH100,GAM,A,Z
    100 FORMAT(3E16.8)
     70 FORMAT(1F10.4,2E10.2)
        IF(SENSE SWITCH 1) 50,51
     50 TYPE70,GAM,A,Z
     51 CONTINUE
C       COMPUTE LEAST-SQUARES SUM
        SLSQ=0.
        DO90 J=1,N
        W=((C(J)-A/(E(J)**GAM))**2)/SIGSQ(J)
     90 SLSQ=SLSQ+W
        PUNCH91,SLSQ
     91 FORMAT(14HLEAST SQ SUM =,F10.2)
        SUM=Z
        ASU=ABS(SUM)
        IF(ASU-.00000001)59,59,57
     59 GO TO 8
     57 CONTINUE
        IF(TEST)61,60,61
```

```
   60 GO TO 30
   61 IF(TEST*SUM)65,63,66
   65 DLT=-DLT/2.
      GO TO 31
   66 CONTINUE
      TEST=ABS(TEST)
      IF(TEST-ASU)62,63,64
   62 DLT=-DLT
      GO TO 31
   63 GO TO 8
   64 GO TO 31
   30 DLT=0.1
   31 GAM=GAM+DLT
      TEST=SUM
      GO TO 10
    8 CONTINUE
      SUMAA=0.
      SUMAB=0.
      SUMBB=0.
      DO24 I=1,N
      EGAM=1./E(I)**GAM
      AA=EGAM**2./SIGSQ(I)
      U=C(I)*EGAM*LOG(E(I))
      V=2.*A*(EGAM**2)*LOG(E(I))
      AB=(U-V)/SIGSQ(I)
      W=C(I)*A*EGAM*(LOG(E(I))**2)
      X=2.*(A*EGAM*LOG(E(I)))**2
      BB=(W-X)/SIGSQ(I)
      SUMAA=SUMAA+AA
      SUMAB=SUMAB+AB
   24 SUMBB=SUMBB+BB
      SUMBB=-SUMBB
      DETH=SUMAA*SUMBB-SUMAB*SUMAB
      SIGA=SQRT(SUMBB/DETH)
      SIGB=SQRT(SUMAA/DETH)
      PUNCH25
   25   FORMAT(41HSTD DEVIATION OF A      STD DEVIATION OF B)
      PUNCH3,SIGA,SIGB
      PUNCH 26
   26 FORMAT(52HENERGY    FIT CURVE    RESIDUALS   DEVIATION IN SIG
      DO27 I=1,N
      CUR=A/E(I)**GAM
      RES=C(I)-CUR
      SIGEV=RES/SQRT(SIGSQ(I))
   27 PUNCH28,E(I),CUR,RES,SIGEV
   28 FORMAT(4F8.1)
      STOP
      END
```

To find the standard deviation of the value of A and the error matrix H_{ij} must be computed, where

$$H = \begin{matrix} H_{AA} & H_{A\gamma} \\ H_{\gamma A} & H_{\gamma\gamma} \end{matrix} .$$

The elements were found to be;

$$H_{AA} = 1/2\ \partial 2M/\partial 2A = \Sigma\ E_i^{-2\gamma}/\sigma_i^2$$

$$H_{A\gamma} = H_{\gamma A} = 1/2\ \partial 2M/\partial A\partial\gamma = -\Sigma\ 1/\sigma_i^2 (C_i E_i^{-\gamma}\ \log E_i\ -2A\ E_i^{-2}\log E_i$$

$$H_{\gamma\gamma} = 1/2\ \partial 2M/\gamma\gamma^2 = -\Sigma\ 1/\sigma_i^2 (C_i\ A\ E_i^{-\gamma}(\ell n E_i)^2\ -2A^2 E_i^{-2\gamma}(\ell n E_i)^2$$

and these are evaluated for the least-squares obtained values of A and γ.

The two standard deviations are formally given by;

$$\sigma_A = \sqrt{H^{-1}_{AA}} ,$$

$$\sigma_\gamma = \sqrt{H^{-1}_{\gamma\gamma}} .$$

The inverse matrix is found from;

$$(H^{-1})_{ij} = (-1)^{j+1}\ \frac{\text{Det(ji minor of H)}}{\text{Det H}} ,$$

so in this case

$$\sigma_A = \sqrt{\frac{H_{\gamma\gamma}}{\det H}} \quad \text{and} \quad \sigma_\gamma = \sqrt{\frac{H_{AA}}{\det H}} ,$$

where Det $H = H_{AA}\ H_{\gamma\gamma} - (H_{A\gamma})^2$.

APPENDIX II.

Data Reduction

The data reduction first involved a play-back of the tape-recorded PCM data. The decoder reconstructed the digital signal from the recorded waveforms; the digital data were stored in the memory of the Nuclear Data analyzer. All PCM data was monitored continuously for spurious noise which sometimes is introduced through RF pickup of such things as ignition noise of vehicles or RF signal drop-out. Any portion of data which contained noise was discarded. The magnetometer channel was monitored on a strip chart recorder to indicate the times at which the azimuth pointing system was switched between North and South.

In this manner blocks of data were recovered and separated into Crab or background observations. These blocks were then separately put onto punched tape by the Nuclear Data and later converted to IBM cards. Each segment of data had associated with it a control card that indicated the time limits of the segment, the altitude and an identification number which identified it as being a Crab or background observation.

To handle the large amount of data which is accumulated during a flight a computer program was written to deal with the most important part of the experiment, the extraction of the spectrum of the Crab Nebula. Some of the general features of the program will be listed below.

From the segments of data previously described the program selects a Crab segment and determines the time

from transit and the zenith angle for the middle of the ten minute observation. Also stored in the program is a list of atmospheric absorption lengths (1/e depths in g/cm^2) compiled for the energy of each of the 127 channels. From the altitude and zenith angle of a particular observation time an atmospheric correction factor for each channel was determined for the slant depth.

The program then selects the two background observation periods adjacent in time to the Crab observation period and averages the two and normalizes it to a time period equal to that of the Crab period under consideration. This averaged background was then subtracted from the Crab observation and a residual was formed. These residuals were then corrected with the previously determined atmospheric absorption factor. The standard deviations for the residuals in each channel were also computed.

This process is carried out for all segments of Crab observation periods. As a final result the total of the residuals for all the observations is multiplied by the experimentally determined detector absorption factors; the corrected total is printed out along with their standard deviations for each of the channels.

ACKNOWLEDGEMENTS:

It is a pleasure to acknowledge the cooperation and guidance of my thesis advisor Dr. R. C. Haymes, who initiated the gamma ray astronomy group at Rice as a result of his inquisitiveness about the nature of the Crab Nebula.

Mr. W. L. Craddock was deeply involved in the design and construction of the balloon-borne system and participated in the initial series of balloon flights which led up to the experiment described. I am also indebted to him for several of the figures used in the text.

Dr. J. D. Kurfess and Dr. W. H. Tucker have provided me with valuable discussions and encouragement. The majority of the electronics were designed and built by Delbert Oehme and Al Heath. J. Fishman, S. Glenn, and J. M. Voss provided assistance before and during the balloon flight and in the reduction of the data. The data reduction program is due to the work of S. Glenn.

The staff of NCAR at Palestine must be commended for their launching and recovery efforts and for all the support they provided during our many stays with them.

This research was sponsored by the Air Force Office of Scientific Research, Office of Space Research by Air Force Grant #AF-AFOSR-858-65 and under Contract #44-620-67-C-0062.

CITATIONS

Anders, E. 1959, Ap. J., 129, 327.

Arnold, J., Metzger, A., Anderson, E., and Van Dilla, M. 1962, J. Geophys. Res., 67, 4878.

Axel, P. 1954, Rev. Sci. Inst., 25, 391.

Bahcall, J., and Wolf, R. 1965 Phys. Rev. Letters, 14, 343.

Becklin, E., 1967 Private communication.

Burbidge, E., Burbidge, G., Fowler, W., and Hoyle, F. 1957, Rev. Mod. Phys., 29, 547.

Burbidge, G., Hoyle, F., Burbidge, E., Christy, R., and Fowler, W. 1956, Phys. Rev., 103, 1145.

Burbidge, G. 1966, in High Energy Astrophysics (L. Gratton, ed.) New York, Academic Press.

Chodil, G., Mark, H., Rodrigues, R., Seward, F., Swift, C., Hiltner, W., Wallerstein, G., and Mannery, E. 1967, Phys. Rev. Letters, 19, 681.

Chubb, T., Friedman, H., and Kreplin, R.1960, J. Geophys. Res., 65, 1831.

Clark, G. 1965, Phys. Rev. Letters, 14, 91.

Clark, G., Lewinn, W., and Smith, W. 1967, Preprint.

Clayton, D. and Craddock, W. 1965, Ap. J., 142, 189.

Craddock, W. 1967, M.S. Thesis, Rice University.

Dolan, J. 1966, Smithsonian Institution Astrophysical Observatory, Research in Space Science, SAO Special Report N212.

Fields, P., Studier, M., Diamond, H., Mech, J., Inghram, M., Pyle, G., Stevens, C., Fried, S., Manning, W., Chiorso, A., Thompson, D., Higgins, G., and Seaborg, G. 1956, Phys. Rev., 102, 180.

Finzi, A. 1965, Phys. Rev. Letters, 15, 599.

Giacconi, R., Gursky, H., Paolini, F., and Rossi, B. 1962, Phys. Rev. Letters, 9, 439.

Gould, R., and Burbidge, G. 1965, Ann. d'Ap., 28, 171.

Grader, R., Hill, R., Seward, F., Toor, A. 1966, Science, 152, 1499.

Gregory, B., and Kreplin, R. 1967, J. Geophys. Res., 72, 4815.

Haymes, R., and Craddock, W. 1966, J. Geophys. Res., 71, 3261.

Heiles, C. 1964, Ap. J., 140, 470.

Hoyle, F., and Fowler, W. 1960, Ap. J., 132, 565.

Hoyle, F., Fowler, W., Burbidge, G., and Burbidge, E. 1964, Ap. J., 139, 909.

Howard, W., and Maran, S. 1965, Ap. J. Supp., X, 193.

Kardashev, N. 1962, Soviet Astronomy-AJ, 6, 317.

Kleinman, D., 1967, Private communication.

Manley, O. 1966, Ap. J., 144, 1253.

Mayall, N. 1962, Science, 137

Melissinos, A. 1966, Experiments in Modern Physics (1st ed., New York: Academic Press), pp. 467-476.

Minkowski, R. 1964, in Annual Review of Astronomy and Astrophysics, ed. by L. Goldberg, (Vol. 2, Palo Alto, Ann. Rev. Inc.), 247.

Morrison, P., and Sartori, L. 1965, Phys. Rev. Letters, 14, 771.

Morrison, P., and Sartori, L. 1966, Phys. Rev. Letters, 16, 414.

Morroz, V. 1964, Soviet Astronomy-AJ, 7, 755.

Neher, H. 1953, Rev. Sci. Inst., 24, 99.

Neher, H., and Johnson, A. 1956, Rev. Sci. Inst., 27, 173.

Neher, H. 1967, J. Geophys. Res., 72, 1527.

Neiler, J. and Bell, P. 1965, in Alpha-, Beta- and Gamma-Ray Spectroscopy (K. Seigbahn, ed.) North-Holland Publishing Co., Amsterdam.

O'Dell, C. 1962, Ap. J., 136, 809.

Oort, J., and Walraven, T. 1956, B.A.N., 12, 285.

Peterson, L., and Winkler, J. 1959, J. Geophys. Res., 64, 697.

Peterson, L., Schwartz, D., Pelling, R., and McKenzie, D. 1966, J. Geophys. Res., 71, 5778.

Peterson, L., Jacobsen, A., and Pelling, R. 1966, Phys. Rev. Letters, 16, 142.

Peterson, L., Jacobsen, A., Pelling, R., and Schwartz, D. 1967, Canad. J. of Phys. (in press).

Sartori, L., and Morrison, P. 1967, Ap. J., 150, 385.

Savedoff, M. 1959, Nuovo Cimento, 13, 12.

Scargle, J. 1967, Astron. Soc. of the Pacific, Leaflet #457.

Shklovskii, I. 1960, Soviet Astronomy-AJ, 4, 355.

Shklovskii, I. 1966, Soviet Astronomy-AJ, 10, 6.

Stein, J., and Lewin, W. 1967, J. Geophys. Res., 72, 383.

Tolbert, C. 1965, Nature, 200, 1304.

Tucker, W. 1967, Ap. J., 148, 745.

U. S. Department of Commerce, Environmental Sciences Service Administration, Boulder, Colorado, Report CRPL-IER-FB-276, Ang. 1967.

Woltjer, L. 1957, B.A.N., 14, 39.

Young, H. 1962, Statistical Treatment of Data (1st ed., New York: McGraw-Hill).